

UC Irvine

UC Irvine Previously Published Works

Title

Mmp14-dependent remodeling of the pericellular–dermal collagen interface governs fibroblast survival

Permalink

<https://escholarship.org/uc/item/2hz2d55x>

Journal

Journal of Cell Biology, 223(9)

ISSN

0021-9525

Authors

Sabeh, Farideh
Li, Xiao-Yan
Olson, Adam W
[et al.](#)

Publication Date

2024-09-02

DOI

10.1083/jcb.202312091

Peer reviewed

ARTICLE

Mmp14-dependent remodeling of the pericellular–dermal collagen interface governs fibroblast survival

Farideh Sabeh¹, Xiao-Yan Li¹, Adam W. Olson¹, Elliot Botvinick², Abhishek Kurup², Luis E. Gimenez³, Jung-Sun Cho¹, and Stephen J. Weiss¹

Dermal fibroblasts deposit type I collagen, the dominant extracellular matrix molecule found in skin, during early postnatal development. Coincident with this biosynthetic program, fibroblasts proteolytically remodel pericellular collagen fibrils by mobilizing the membrane-anchored matrix metalloproteinase, Mmp14. Unexpectedly, dermal fibroblasts in *Mmp14*^{-/-} mice commit to a large-scale apoptotic program that leaves skin tissues replete with dying cells. A requirement for Mmp14 in dermal fibroblast survival is recapitulated in vitro when cells are embedded within, but not cultured atop, three-dimensional hydrogels of crosslinked type I collagen. In the absence of Mmp14-dependent pericellular proteolysis, dermal fibroblasts fail to trigger β 1 integrin activation and instead actuate a TGF- β 1/phospho-JNK stress response that leads to apoptotic cell death in vitro as well as in vivo. Taken together, these studies identify Mmp14 as a requisite cell survival factor that maintains dermal fibroblast viability in postnatal dermal tissues.

Introduction

Dermal fibroblasts constitute a functionally and transcriptionally unique population of mesenchymal cells that play key roles in regulating the development and maintenance of skin, the largest integument in mammals (Driskell and Watt, 2015; Rognoni and Watt, 2018). From a structural perspective, dermal fibroblasts are responsible for synthesizing and depositing type I collagen, the dominant extracellular protein found within the dermis (Driskell and Watt, 2015; Rognoni and Watt, 2018). Triple-helical in nature, type I collagen fibrils assume a liquid crystal-like structure that confers skin with its mechanical strength, while maintaining its malleable characteristics (Orgel et al., 2006; Perumal et al., 2008). Type I collagen also regulates the cellular functions of embedded fibroblasts, adipocytes, vascular networks, and nerves via integrin- and non-integrin-type receptors that are linked to complex mechanotransduction pathways (Grinnell and Petroll, 2010).

Consistent with its major roles in defining tissue structure and function, type I collagen is highly resistant to most forms of proteolytic attack (Fields, 2013). Nevertheless, type I collagen undergoes purposeful proteolytic remodeling during a range of tissue reparative and pathologic events, including wound healing, aging, and cancer (Ewald et al., 2015; Fields, 2013; Rowe and Weiss, 2009).

Indeed, dermal fibroblasts are able to mobilize significant collagenolytic activity as a consequence of their ability to express metalloproteinases that are capable of hydrolyzing triple-helical collagen (Sabeh et al., 2004, 2009a). Interestingly, dermal collagen undergoes selective degradation during early postnatal growth (Klein and ChandraRajan, 1977), but the proteolytic enzymes responsible for this activity have not been defined nor has the functional significance of collagenolysis on dermal development been characterized.

In an effort to define the proteolytic mechanisms responsible for the dermal fibroblast-mediated remodeling of the pericellular type I collagen network during early postnatal development, we examined fibroblast function in mice selectively deficient in each of the major collagenolytic enzymes expressed in the murine genome, i.e., Mmp2, Mmp8, Mmp13, Mmp14, Mmp15, and Mmp16 (Fields, 2013). Herein, we demonstrate that the pericellular collagenase, Mmp14/MT1-MMP, alone plays a required role in dermal collagen remodeling. Following Mmp14 knockout, an unusual dermal phenotype develops marked by widespread dermal fibroblast apoptosis that is characterized by an impaired activation of β 1 integrin-linked signaling cascades. Consequently, the inability to accommodate the mechanotransduction pathways linked to the normal remodeling of the

¹Division of Genetic Medicine, Department of Internal Medicine, Life Sciences Institute, University of Michigan, Ann Arbor, MI, USA; ²The Henry Samueli School of Engineering, University of California, Irvine, CA, USA; ³Life Sciences Institute, University of Michigan, Ann Arbor, MI, USA.

Correspondence to Stephen J. Weiss: sjweiss@umich.edu.

© 2024 Sabeh et al. This article is distributed under the terms of an Attribution–Noncommercial–Share Alike–No Mirror Sites license for the first six months after the publication date (see <http://www.rupress.org/terms/>). After six months it is available under a Creative Commons License (Attribution–Noncommercial–Share Alike 4.0 International license, as described at <https://creativecommons.org/licenses/by-nc-sa/4.0/>).

3-D dermal matrix activates a TGF- β 1–JNK signaling cascade that triggers fibroblast death in vitro as well as in vivo. Taken together, these studies identify a heretofore unrecognized, *Mmp14*-mediated fibroblast prosurvival network that is dependent on the dynamic remodeling of the dermal type I collagen network.

Results

Mmp14 deficiency promotes fibroblast apoptosis in vivo

In vivo, dermal fibroblasts of 1-mo-old mice are embedded in a dense matrix of type I collagen fibrils, a portion of which has undergone proteolytic degradation as detected by a monoclonal antibody specific for collagenase-dependent hydrolysis (Fig. 1, A–C) (Tang et al., 2022). Consistent with recent studies indicating the pericellular collagenase, *Mmp14*, is expressed in type I collagen-rich tissues in vivo (Chun et al., 2006; Feinberg et al., 2018; Hotary et al., 2003; Tang et al., 2013), *Mmp14* is detected in fibroblast populations found throughout the dermis, including the papillary and reticular zones (Driskell and Watt, 2015), as assessed by β -galactosidase staining of tissues recovered from *Mmp14^{+/lacZ}* knock-in mice and confirmed by western blot (Fig. 1 D). Further, in keeping with its demonstrated type I collagenolytic activity in vivo (Chun et al., 2006; Feinberg et al., 2018; Tang et al., 2013), few, if any, collagen degradation products are detected by immunostaining in *Mmp14^{-/-}* skin (Fig. 1 C).

Using transmission electron microscopy (TEM) to assess the impact of *Mmp14* targeting on dermal architecture, we unexpectedly noted tissue fields heavily populated with dead fibroblasts containing fragmented nuclei in tandem with TUNEL- and caspase-3–positive cells (Fig. 1 E). Underlining the specificity of this proapoptotic effect on dermal tissues, we have previously noted that increased apoptosis is not detected in other fibroblast-populated tissues, including mammary stroma, lungs, tendons/ligaments, or bones (Feinberg et al., 2016, 2018; Tang et al., 2013). While *Mmp14* targeting has been reported to trigger cell senescence in vivo (Gutiérrez-Fernández et al., 2015), no increases are detected in knockout dermal tissues relative to wild-type controls (Fig. S1). Finally, while both the secreted MMPs, *Mmp2*, *Mmp8*, and *Mmp13*, as well as the membrane-anchored MMPs, *Mmp15* and *Mmp16*, have been reported to cleave type I collagen (Fields, 2013) and are expressed by dermal fibroblasts (Table S1), global knockouts of each these proteinases does not alter collagen deposition or trigger apoptotic responses (Fig. 1, F and G).

A cell-autonomous 3-D–specific survival role for fibroblast *Mmp14*

While our results are consistent with a cell-autonomous defect, fibroblast survival can potentially be modulated by interactions with surrounding keratinocytes, adipocytes, or endothelial cells as well as the extracellular matrix (ECM) itself (Driskell and Watt, 2015). To determine whether *Mmp14* exerts a cell-autonomous survival effect, wild-type or *Mmp14^{-/-}* dermal fibroblasts were isolated and cultured in vitro and apoptosis was monitored. When cultured atop type I collagen gels under 2-D culture conditions, *Mmp14^{+/+}* and *Mmp14^{-/-}* fibroblasts assume indistinguishable morphologies (Fig. 2 A). Similarly, despite reports of cytoskeletal and nuclear defects in *Mmp14^{-/-}* fibroblasts cultured in 2-D

(Gutiérrez-Fernández et al., 2015), no apparent changes were detected in actin or vimentin organization, nuclear lamin A/C levels, senescence markers, and DNA damage or apoptosis relative to wild-type controls (Fig. S2, A–G).

While *Mmp14^{-/-}* fibroblasts cultured under 2-D conditions in vitro fail to recapitulate the in vivo phenotype marked by increased cell death, fibroblasts display distinct phenotypic and functional characteristics when embedded within—rather than cultured atop—a 3-D ECM (Grinnell and Petroll, 2010; Sabeh et al., 2004). As such, *Mmp14^{+/+}* or *Mmp14^{-/-}* fibroblasts were next cultured within 3-D type I collagen gels, and as described previously (Grinnell et al., 2003), within 8 h of 3-D culture, wild-type fibroblasts adopt a characteristic dendritic morphology (Fig. 2 A). By 48 h, the *Mmp14^{+/+}* fibroblasts assume a stable, stellate morphology that is maintained over the 5-day culture period (Fig. 2 A). In concert with these changes, wild-type fibroblasts actively remodel the surrounding collagen matrix, leaving distinct zones of hydrolytic “clearing” in the pericellular environment as assessed by scanning electron microscopy (SEM)—an event likewise marked by active collagenolysis where collagen fragments appear in both the pericellular and intracellular environments (Fig. 2 B) (Madsen et al., 2007).

Similar to wild-type fibroblasts, *Mmp14^{-/-}* fibroblasts also adopt a dendritic shape in the early phases of 3-D culture, but in contrast to *Mmp14^{+/+}* cells, the null fibroblasts remain “locked” in a dendritic shape with distinct blebbing (Fig. 2 A and Fig. S2 H). Under these conditions, *Mmp14^{-/-}* fibroblasts are unable to degrade the surrounding collagen matrix (Fig. 2 B). Significantly, by 48 h in 3-D culture, *Mmp14^{-/-}* fibroblasts are surrounded by membrane vesicles suggestive of an apoptotic event whose induction is confirmed by both caspase-3 activation and TUNEL staining in a fashion similar to that observed in vivo (Fig. 2, C and D). While papillary and reticular fibroblasts can express distinct activities in vivo and in vitro (Driskell and Watt, 2015), either population isolated from *Mmp14^{-/-}* mice, but not control littermates, likewise undergoes comparable cell death in vitro (Fig. 2, E and F). Finally, consistent with the induction of programmed cell death, both caspase-3 activity and apoptosis are suppressed to background levels when *Mmp14^{-/-}* fibroblasts are cultured in the presence of the pan-caspase inhibitor, Z-VAD fluoromethylketone (Fig. 2, C and D) (Nicholson, 2000).

Structure/function analysis of *Mmp14*-dependent prosurvival activity at the fibroblast collagen interface

As *Mmp14^{-/-}* fibroblasts are recovered from global knockout mice with multiple phenotypic defects (Gutiérrez-Fernández et al., 2015; Holmbeck et al., 1999; Zhou et al., 2000), the cells could potentially retain a mechanical “memory” of their in vivo setting (Lee et al., 2014; Yang et al., 2014). To determine whether null fibroblasts recover normal function following re-expression of wild-type *Mmp14*, null cells were transduced with control or *Mmp14* lentiviral expression vectors and embedded in 3-D collagen. Under these conditions, normal cell morphology is regained following re-expression of *Mmp14*, while apoptosis falls to wild-type levels (Fig. 3, A and B; and Fig. S3 A). Conversely, dermal fibroblasts recovered from *Mmp14^{fl/fl}* mice and transduced with an adenoviral-Cre expression vector in vitro undergo

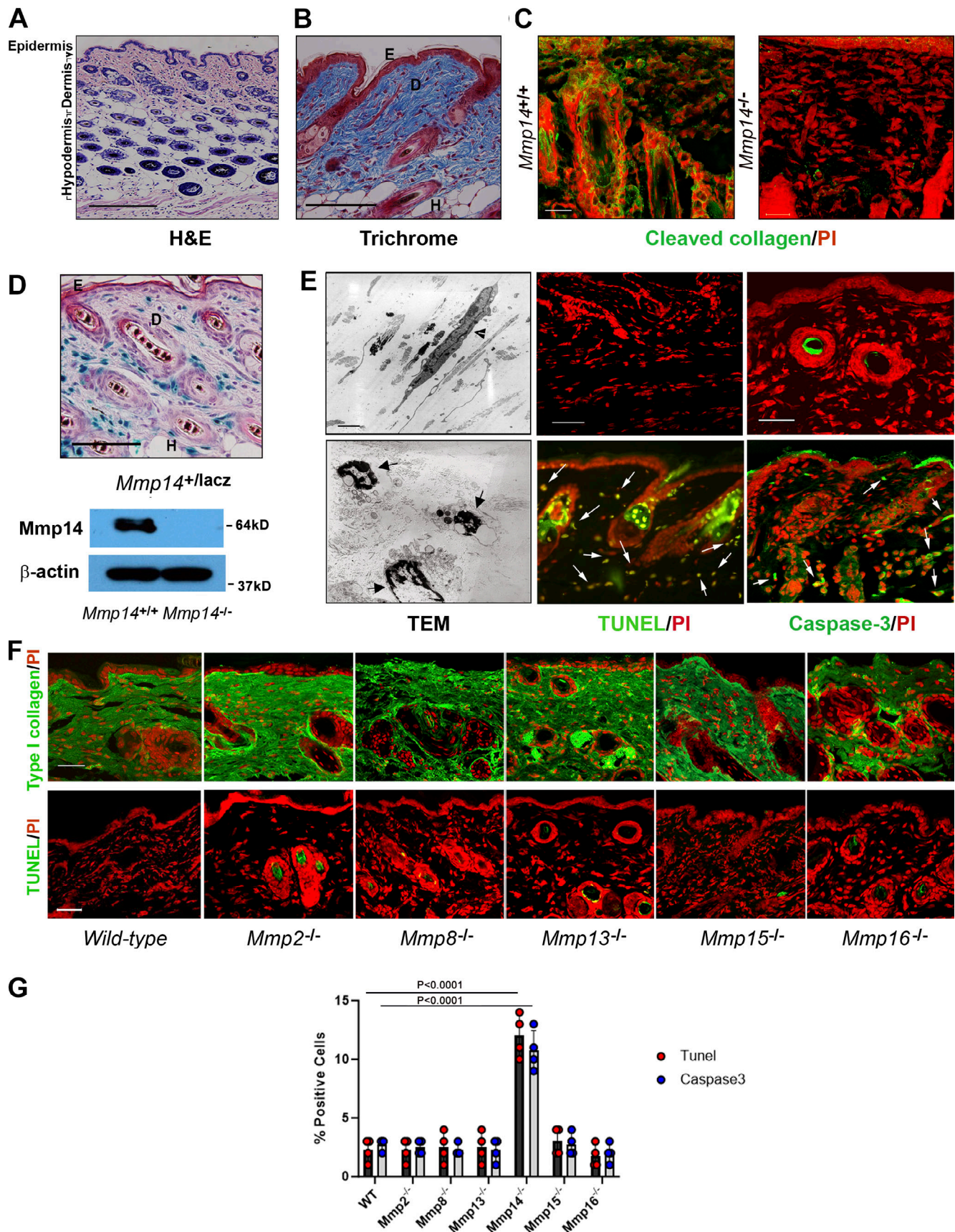


Figure 1. **Mmp14-dependent control of dermal fibroblast viability.** (A and B) Cross-sections of dorsal skin from 4-wk-old wild-type mice. Tissues were stained with either H&E (A) or Trichrome (B). Bar = 100 μ m. (C) Cleaved collagen was visualized in wild-type or *Mmp14^{-/-}* by immunofluorescence (bar = 25

μm). Results representative of three experiments performed. **(D)** Cross-section of dorsal skin from 4-wk-old *Mmp14^{+/-lacZ}* processed for β-galactosidase activity with *Mmp14* protein levels assessed by western blot (bar = 100 μm). E, epidermis; D, dermis; and H, hair follicle. **(E)** Skin isolated from 4-wk-old *Mmp14^{+/+}* or *Mmp14^{-/-}* mice was fixed for TEM with live/dead fibroblasts indicated by arrowheads and arrows, respectively (bar = 2 μm), or stained for either active caspase-3 or TUNEL with PI counterstaining (positive cells are marked by arrows). Bar = 50 μm. TEM results are representative of two independent experiments performed while staining results are representative of three independent experiments performed. **(F)** Representative type I collagen immunostaining and TUNEL staining with nuclei counterstained red with PI of dorsal skin harvested from 4-wk-old wild-type mice versus that of *Mmp2^{-/-}*, *Mmp8^{-/-}*, *Mmp13^{-/-}*, *Mmp15^{-/-}*, and *Mmp16^{-/-}* mice. Bar = 100 μm. Results representative of three independent experiments performed. **(G)** Percent TUNEL- and caspase-3-positive cells in dermal tissues recovered from dorsal skin of 4-wk-old wild-type and *Mmp14* knockout mice. Results are expressed as the mean ± SEM of four independent experiments with P values determined by one-way ANOVA and Dunnett's post-test. Source data are available for this figure: SourceData F1.

apoptosis in 3-D culture following acute deletion of the floxed alleles (Fig. S3, B and C). While these results demonstrate that fibroblasts require *Mmp14* to maintain 3-D survival, recent studies indicate that the enzyme can alter cell function by either proteinase-dependent or -independent effects (Gonzalo et al., 2010; Sakamoto et al., 2014; Tang et al., 2013). Nevertheless, following transduction with a catalytically inactive form of MMP14, MMP14 E240A (MMP14_{E/A}), *Mmp14^{-/-}* fibroblasts continue to display defects in cytoskeletal remodeling and reduced cell survival in 3-D culture (Fig. 3 B and Fig. S3 A). Similar results are observed when MMP14_{E/A}-transduced null fibroblasts are incubated with the endogenous MMP inhibitor, TIMP-2, to generate a proteinase-inhibitor complex that has been reported to exert prosurvival effects in 2-D culture (Fig. 3, A and B; and Fig. S3 A) (Valacca et al., 2015). By contrast, TIMP-2, a potent inhibitor of *Mmp14* catalytic activity (Zucker et al., 1998), readily induces apoptotic responses when added in supraphysiologic levels to wild-type fibroblasts in 3-D culture (Fig. S3, A and C).

As these results support a model wherein proteolytically active *Mmp14* controls cell survival, we sought to identify the critical structural determinants that underlie its ability to regulate cell survival. Consistent with recent studies demonstrating that *Mmp14*-dependent collagenolytic activity is retained when cells are transduced with MMP14 mutants where the cytosolic tail (MMP14 ΔCT) or hemopexin domain (MMP14 ΔHPX) are deleted (Sabeh et al., 2009a; Sakr et al., 2018), each of these constructs rescue *Mmp14^{-/-}* fibroblast morphology and viability defects (Fig. 3, A and B; and Fig. S3 A). Further, despite the fact that the mouse genome does not encode an ortholog of the dominant human collagenase, MMP-1 (Sabeh et al., 2009a), when the catalytic domain of MMP14 is replaced with that of the secreted human collagenase, MMP-1 (MMP14_{MMP-1CAT}), in either the presence or absence of the MMP14 hemopexin domain, (i.e., MMP14_{MMP-1CAT/ΔHPX}), the transduced *Mmp14^{-/-}* fibroblasts retain viability in 3-D culture (Fig. 3, A and B; and Fig. S3 A). By contrast, if MMP14 is expressed as a transmembrane-deletion mutant (i.e., MMP14 ΔTM), the enzymatically active, but secreted proteinase, no longer rescues the proapoptotic behavior of the transduced *Mmp14^{-/-}* fibroblasts (Fig. 3, A and B; and Fig. S3 A). Hence, the prosurvival activity of *Mmp14* is linked directly to its ability to act as a membrane-tethered collagenase.

Type I collagenolysis and the induction of fibroblast shape change-dependent apoptosis

A requirement for *Mmp14*-dependent pericellular collagenolysis in maintaining fibroblast survival is potentially consistent with

earlier studies that assigned antiproliferative or proapoptotic roles to native type I collagen fibrils (Birukawa et al., 2014; Koyama et al., 1996; Montgomery et al., 1994; Wall et al., 2007; Zhou et al., 2006). In these models, cell-mediated collagenolysis not only inactivates the growth-suppressive signals assigned to type I collagen but also generates collagen fragments that trigger prosurvival responses (Birukawa et al., 2014; Koyama et al., 1996; Montgomery et al., 1994; Wall et al., 2007; Zhou et al., 2006). Alternatively, collagen networks may induce cell death responses by confining fibroblasts in a cage-like network of fibrils that prevent the cell shape changes or tractional forces normally associated with 3-D survival (Folkman and Moscona, 1978; Wang et al., 2000). To discriminate between these models, *Mmp14^{-/-}* fibroblasts were embedded in 3-D hydrogels constructed from reductively alkylated collagen trimers that are unable to form the intermolecular, Schiff-base crosslinks that define collagenous networks in vivo (Sabeh et al., 2009b). Hydrogels formed from the borohydride-reduced collagen retain near-normal rigidity and pore size (i.e., for native collagen gels, $G' = 118 \pm 12$ Pa with a pore size of 1.3 ± 0.6 μm versus 84 ± 5 Pa and 1.3 ± 0.8 μm for reduced collagen; mean ± SEM, $n = 55$ individual point determinations). However, in contrast with native collagen hydrogels, *Mmp14*-null cells embedded in non-crosslinked collagen hydrogels remain fully viable in either the absence or presence of TIMP-2, reflecting the inability of collagen networks to induce cell death independently of its normally crosslinked network structure (Fig. 3, C and D). Similar results are obtained if collagen gels are prepared from pepsin-treated monomers (Sabeh et al., 2009b) where the non-helical telopeptides that normally harbor the aldimine crosslinks are removed (Fig. 3, C and D). As these results suggest that *Mmp14*-dependent survival operates independently of the hydrogel molecular composition per se (i.e., as opposed to its structural/mechanical properties), we sought to determine whether wild-type fibroblasts could be induced to undergo apoptosis when shape-constrained in a synthetic hydrogel that precludes proteolytic remodeling (Tang et al., 2013). As such, wild-type or null fibroblasts were embedded in polyethylene glycol (PEG)-based hydrogels that are decorated with proadhesive integrin ligands and crosslinked with short peptides that do—or do not—contain *Mmp14*-hydrolyzeable bonds. As expected, *Mmp14^{+/+}* fibroblasts undergo normal shape changes in the proteinase-sensitive hydrogel and maintain viability (Fig. 3, D and E). By contrast, wild-type cells are only able to extend small dendritic processes in the non-hydrolyzable gel—an event that coincides with markedly up-regulated apoptosis (Fig. 3, D and E). In turn, *Mmp14^{-/-}* fibroblasts fail

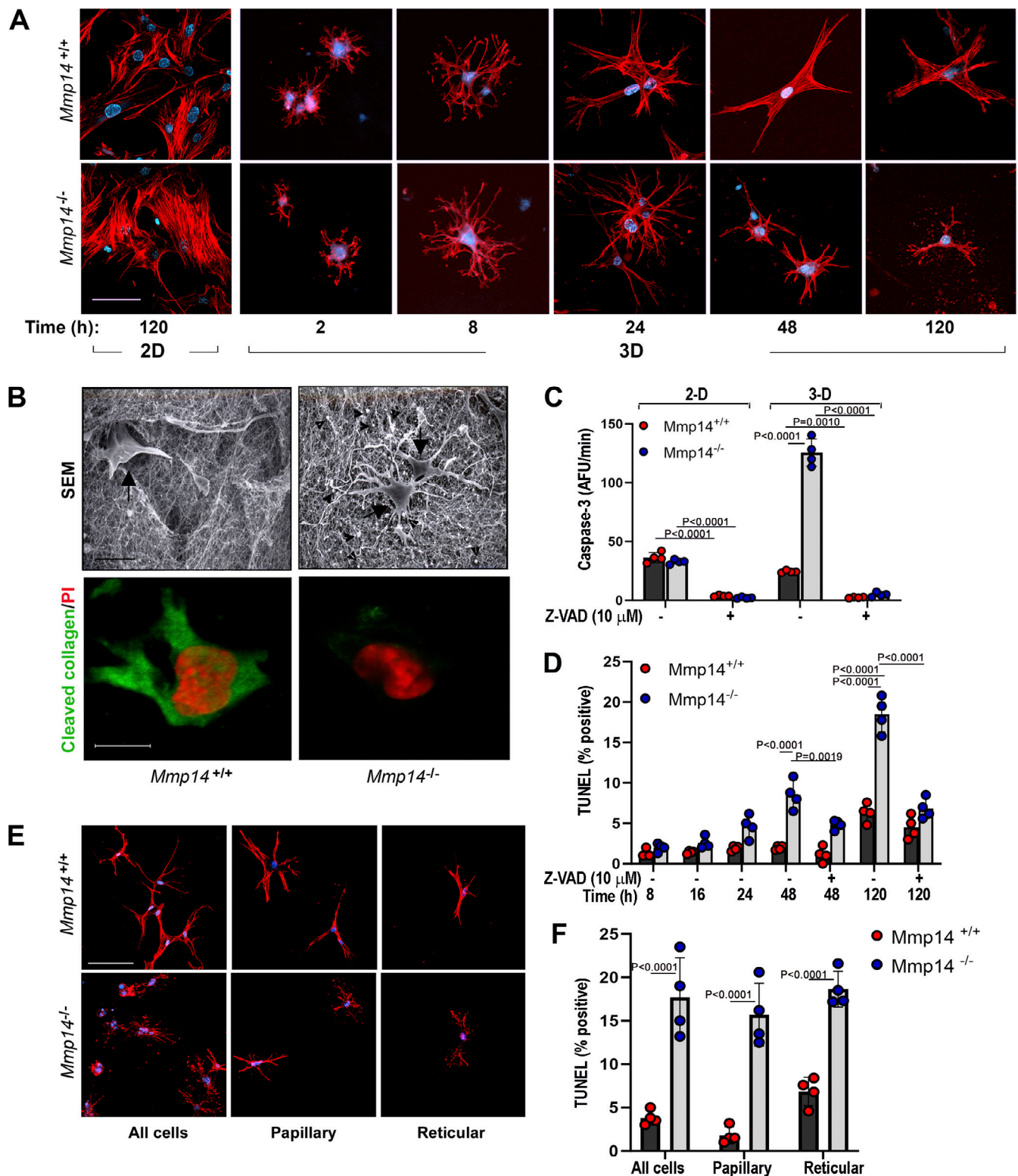


Figure 2. **Regulation of cell shape and survival by Mmp14 in 3-D culture.** (A) Dermal fibroblasts isolated from newborn *Mmp14*^{+/+} or *Mmp14*^{-/-} mice were cultured atop (2-D) or embedded within (3-D) type I collagen hydrogels for 2–120 h, fixed and stained for F-actin (phalloidin) with nuclear counterstaining (DAPI). Wild-type and knockout fibroblasts in 2-D culture are indistinguishable at the 120-h time point. In 3-D culture, wild-type and *Mmp14*-null fibroblasts display divergent shape changes with *Mmp14*^{-/-} cells shedding F-actin-positive vesicles (bar = 100 μ m). Results are representative of three independent experiments performed. (B) *Mmp14*^{+/+} or *Mmp14*^{-/-} fibroblasts were embedded in 3-D collagen hydrogels for 120 h, fixed, and the cell–collagen interface visualized by SEM (bar = 10 μ m) with pericellular collagen degradation products identified by immunofluorescence with anti-cleaved type I collagen antibody (bar = 20 μ m). Results are representative of two independent experiments performed. (C) Caspase-3 activity of *Mmp14*^{+/+} versus *Mmp14*^{-/-} fibroblasts cultured atop (2-D) or embedded within (3-D) type I collagen hydrogels in the absence or presence of 10 μ M Z-VAD (mean \pm SEM; *n* = 4 independent experiments) with

P values determined by two-way ANOVA and Tukey post-test. AFU, active fluorescent units. **(D)** Time-dependent increase in TUNEL staining in *Mmp14*^{+/-} versus *Mmp14*^{-/-} fibroblasts cultured in the absence or presence of 10 μ M Z-VAD (mean \pm SEM; $n = 4$ independent experiments) with P values determined by two-way ANOVA and Tukey post-test. **(E and F)** Fibroblasts were isolated from newborn *Mmp14*^{+/-} or *Mmp14*^{-/-} skin and embedded in type I collagen hydrogels as either an unsorted population (all cells) or following FACS into papillary or reticular fibroblast fractions. Following a 5-day culture period, cells were stained for F-actin with DAPI counterstaining (bar = 100 μ m) (E) or TUNEL-stained and quantified (F) (mean \pm SEM; $n = 4$ independent experiments) with P values determined by two-way ANOVA and Tukey post-test.

to undergo shape changes in either the *Mmp14*-sensitive or -insensitive hydrogel format and display an apoptotic phenotype similar to that observed when wild-type fibroblasts are entrapped in the protease-resistant hydrogel (Fig. 3, D and E). Hence, *Mmp14*-dependent prosurvival effects are linked directly to cell shape changes arising as a consequence of the cell's ability to dissolve physically constraining structural barriers.

Postnatal patterns of dermal collagen expression regulate fibroblast apoptosis

Despite a requirement for the dynamic proteolytic remodeling of the type I collagen–dermal fibroblast interface in vivo, a conundrum exists wherein neonatal wild-type and *Mmp14*-null animals are virtually indistinguishable at birth (Holmbeck et al., 1999; Zhou et al., 2000). Marked changes in postnatal development only begin at P4–5, with major changes in body weight, size, and skeletal development developing between 1 and 2 wk of age (Holmbeck et al., 1999; Zhou et al., 2000). Interestingly, when examining fibroblast apoptosis as a function of age, increases in fibroblast apoptosis in *Mmp14*^{-/-} mice are similarly delayed with significant changes only beginning between P7 and P14 (Fig. 4, A and B). In considering potential mechanisms whereby *Mmp14*-null fibroblasts bypass cell death in early postnatal development, we noted that the murine ECM, particularly with regard to type I collagen levels and cross-linking, undergoes major changes in composition and structure over the first 3 wk of postnatal life (Butzow and Eichhorn, 1968; Carver et al., 1993; Kalson et al., 2015; Mao et al., 2002; Mays et al., 1988). Indeed, dermal tissues harvested from either newborn wild-type or *Mmp14*^{-/-} mice contain virtually undetectable levels of type I collagen that subsequently increase as a function of age (Fig. 4, A and C). Furthermore, increases in collagen content correlate with rising levels of apoptosis in *Mmp14*^{-/-}, but not *Mmp14*^{+/-} fibroblasts (Fig. 4, A–C). Though *Mmp14* activity has been reported to regulate type I collagen fibril release from cell surfaces (Taylor et al., 2015), dermal collagen fibril size and levels are normal in the dermal tissues of *Mmp14*^{-/-} mice relative to wild-type controls (Fig. S4).

Having established a correlation between the onset of type I collagen deposition and dermal fibroblast apoptosis *Mmp14*-null animals, we sought to determine whether type I collagen content directly defines a requirement for *Mmp14* activity in vivo. As such, *Mmp14*^{+/-} or *Mmp14*^{-/-} fibroblasts were isolated from dermal explants of neonatal mice, labeled with fluorescent microbeads, and injected intradermally into skin explants recovered from 1-, 7-, 14-, or 28-day-old wild-type mice. Explants were then maintained in a viable state by culturing the recombined tissues atop the chorioallantoic membrane of live chick embryos (Sabeh et al., 2009b). While injected wild-type fibroblasts remain

viable in each dermal explant—independent of its age—*Mmp14*^{-/-} fibroblasts only maintain viability in 1-day-old explants with apoptosis levels increasing steadily to >30% when implanted in 28-day-old, wild-type tissues (Fig. 4, C and D). Finally, to establish whether type I collagen levels alone directly and differentially affect fibroblast survival, wild-type or null cells were embedded in 3-D hydrogels whose type I collagen concentration ranges from 0.5 to 3.5 mg/ml. Consistent with our in vivo observations, apoptosis levels increase markedly in *Mmp14*-null, but not wild-type populations, as type I collagen concentrations rise above 0.5 mg/ml (Fig. 4, F and G). Hence, the prosurvival effects afforded by *Mmp14* in vitro or in vivo are type I collagen dependent, allowing *Mmp14*^{-/-} dermal fibroblasts to avoid cell death triggers until collagen levels increase in the early postnatal period.

An *Mmp14*-linked β 1 integrin signaling cascade impacts dermal fibroblast survival

To identify signaling pathways that are dysregulated in *Mmp14*-targeted fibroblasts, wild-type and null cells were embedded in 3-D collagen for 48 h (a time point where minimal apoptosis is observed), and RNA harvested for next-generation sequencing. Under these conditions, almost 600 transcripts were differentially expressed (Fig. 5 A). Interestingly, gene set enrichment analysis identified alterations in transcripts associated with focal adhesions, PI3K/Akt signaling, and cell adhesion and migration (Fig. 5 B). Consistent with these results, whereas collagen-embedded wild-type fibroblasts activate β 1 integrin, phosphorylate FAK, and increase Rho-GTP levels, each of these responses is markedly depressed in the null fibroblasts with Rho-GTP levels falling to 2% of control ($n = 2$; Fig. 5, C and D). To define the relative importance of defective β 1 integrin signaling in the apoptotic phenotype displayed by *Mmp14*^{-/-} fibroblasts, knock-out cells were transduced with a constitutively active, G429N β 1 integrin mutant (Tang et al., 2013) and embedded in 3-D collagen hydrogels. Importantly, the active β 1 integrin mutant fully reversed apoptosis and caspase-3 activation to wild-type levels (Fig. 5, E and F).

TGF- β 1-induced JNK activation triggers dermal fibroblast cell death in vitro and in vivo

In addition to changes in β 1 integrin signaling, apoptosis may also be triggered by changes in matrix rigidity that, in turn, function as an upstream regulator of integrin activation itself (e.g., Leight et al., 2012). As the cytoskeletal-mediated contractile activity of collagen-embedded cells can modulate the mechanical properties of the surrounding matrix (Han et al., 2018), we next used optical tweezer-based active microrheology to monitor rigidity changes taking place at distances both near and far from wild-type and null fibroblast in 3-D culture (Tang et al.,

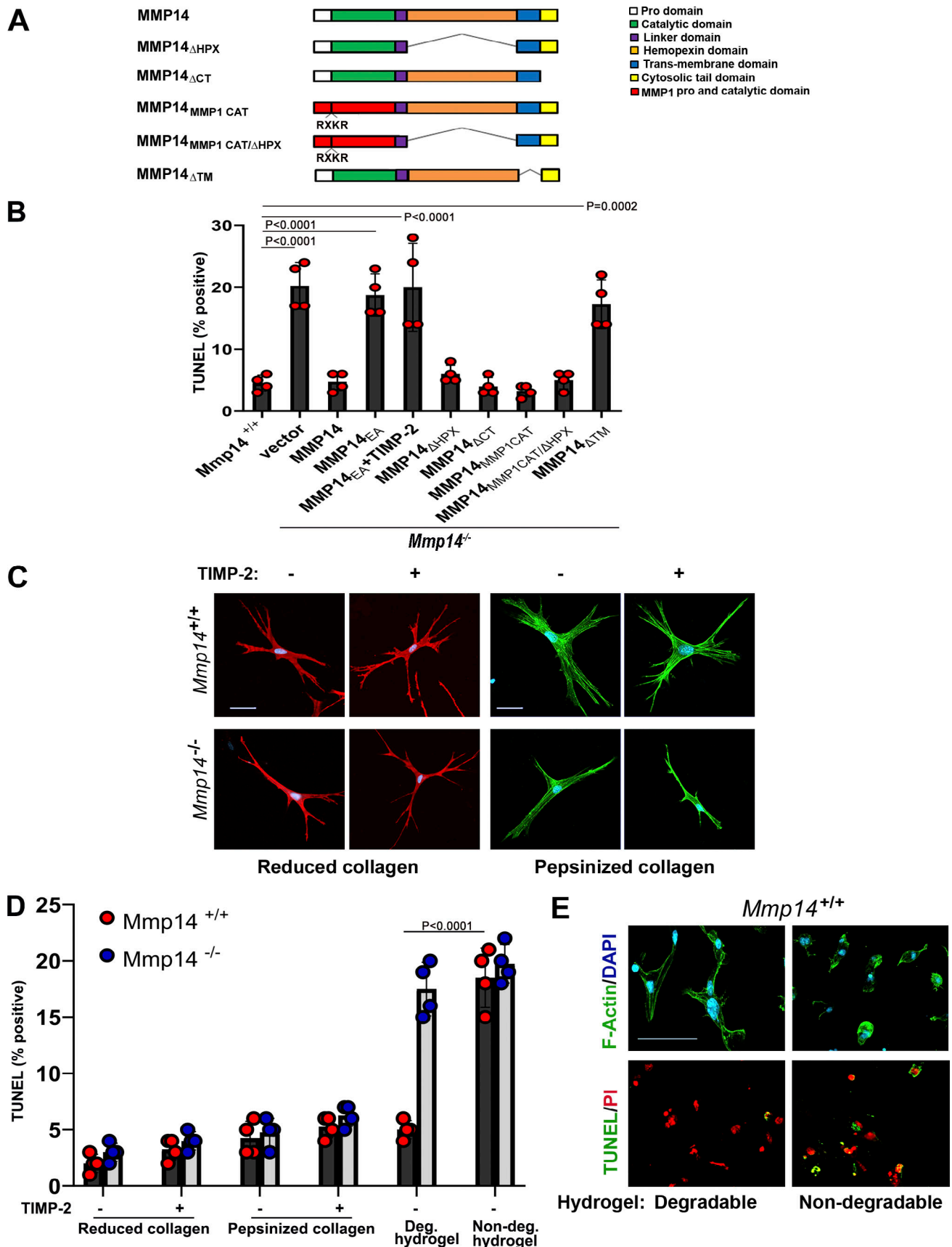


Figure 3. **Mmp14-dependent pericellular proteolysis and the regulation of fibroblast survival.** (A) Schematic diagram of *Mmp14* with prodomain, an RXKR-furin recognition sequence that directs proenzyme activation, catalytic, linker, hemopexin, transmembrane as well as cytosolic tail domains highlighted.

MMP14 mutants were engineered with an inactivating point mutation (E240→A) inserted in the catalytic domain (MMP14_{EA}), the hemopexin or cytosolic tail deleted (i.e., MMP14_{ΔHPX} and MMP14_{ΔCT}), the MMP14 pro- and catalytic domains replaced with the pro- and catalytic domains of human MMP-1 wherein an RXKR sequence was inserted at the terminus of the pro-domain and the MMP14 hemopexin domain retained or deleted (i.e., MMP14_{MMP-1CAT} and MMP14_{MMP1/CAT/ΔHPX}) or the MMP14 transmembrane and cytosolic tail deleted (i.e., MMP14_{ΔTM}). **(B)** *Mmp14*^{-/-} fibroblasts were transduced with control, wild-type MMP14, or mutant MMP14 constructs, embedded in 3-D collagen hydrogels, and cultured for 5 days in the absence or presence of TIMP-2 (3 μg/ml). TUNEL-positive cells were then enumerated (mean ± SEM; n = 4 independent experiments) with P values determined by one-way ANOVA and Tukey post-test. **(C and D)** *Mmp14*^{+/+} or *Mmp14*^{-/-} fibroblasts were embedded in 3-D type I collagen hydrogels prepared from borohydride-reduced or pepsin-hydrolyzed collagen trimers and cultured for 5 days in the absence or presence of TIMP-2 (3 μg/ml). Cells were then phalloidin-stained with DAPI counterstaining (C) (bar = 50 μm) and the percent TUNEL-positive fibroblasts determined in D (mean ± SEM; n = 4 independent experiments) with P values determined by two-way ANOVA and Tukey post-test. **(E)** *Mmp14*^{+/+} or *Mmp14*^{-/-} fibroblasts were embedded in *Mmp14*-degradable or non-degradable PEG-based hydrogels for 5 days and then stained for F-actin and TUNEL (bar = 50 μm). The percentage of TUNEL-positive cells is shown in panel D (mean ± SEM; n = 4 independent experiments).

2013). While the local rigidity of the collagen matrix surrounding *Mmp14*^{+/+} fibroblasts increases almost sixfold to 200 Pa, that surrounding *Mmp14*^{-/-} fibroblasts only doubles (Fig. 6 A). Nevertheless, changes in matrix rigidity alone are not necessarily sufficient to induce apoptotic responses. Recent studies demonstrated that soft matrices sensitized cells to apoptotic responses but only in the presence of TGF-β1 (Leight et al., 2012). In this regard, plasma levels of TGF-β1 are markedly increased in *Mmp14*^{-/-} mice (Gutiérrez-Fernández et al., 2015; Leight et al., 2012). Consistent with this report, TGF-β1 transcripts are up-regulated more than threefold in *Mmp14*-null fibroblasts embedded in type I collagen hydrogels, with attendant increases in both total and active TGF-β1 protein levels (Fig. 6, B and C). To determine whether increases in active TGF-β1 levels alter TGF-β signaling, 3-D-embedded wild-type and *Mmp14*-null fibroblasts were probed for changes in canonical versus non-canonical signaling as monitored by phospho-SMAD2 (pSMAD2) or mitogen-activated protein kinase levels (Massague, 2012). Under these conditions, *Mmp14*^{-/-} fibroblasts express increased levels of p-SMAD2, but neither phospho-ERK (pERK) nor phospho-p38 levels are affected (Fig. 6 D). By contrast, the levels of the p54 and p46 isoforms of phospho-JNK1,2 (pJNK) levels are increased relative to wild-type fibroblasts when *Mmp14*^{-/-} fibroblasts are embedded in native, but not pepsin-extracted, collagen hydrogels (Fig. 6 E). Of note, the JNK inhibitor, SP600125 (Lee and Schiemann, 2011), inhibits increased levels of pJNK (Fig. 6 F) while no changes in pJNK levels between wild-type and null fibroblasts are detected in 2-D culture (Fig. S5, A and B).

As TGF-β-JNK signaling is activated under stress conditions that trigger apoptotic responses in other cell systems (Lee and Schiemann, 2011; Lei et al., 2002; Schuster et al., 2002; Wang et al., 2007), we next assessed the effects of TGF-β neutralizing antibodies or SP600125 on the proapoptotic phenotype of *Mmp14*^{-/-} fibroblasts. Indeed, in the presence of anti-TGF-β neutralizing antibodies or SP600125, all cell death markers including caspase-3 activation and apoptosis are blocked (Fig. 6, G and H). By contrast, the MEK1/2 inhibitor, PD325901, did not abrogate cell death programs in *Mmp14*-null fibroblasts (Fig. 6, G and H). While apoptosis levels in *Mmp14*^{-/-} fibroblasts are further increased by supplementing 3-D cultures with exogenous TGF-β1, wild-type fibroblasts are, as predicted, resistant to the proapoptotic effects of TGF-β1 and maintain full viability (Fig. S5, C and D).

Finally, we returned to *Mmp14*^{-/-} mice to determine whether combined defects in β1 integrin activation and JNK activation could be identified in vivo. Indeed, as observed in vitro,

β1 integrin activation, as well as Rho-GTP levels (11% of control values; n = 2), are strongly repressed in *Mmp14*^{-/-} dermal tissues (Fig. 7, A-C). Further, pJNK levels are increased in *Mmp14*^{-/-} dermal tissues relative to wild-type controls in tandem with the expected marked increases in TUNEL-positive cells (Fig. 7, D-F; and Fig. S5 E). However, when *Mmp14*^{-/-} mice were treated with either anti-TGF-β antibodies or SP600125 during the first 3 wk of life, increases in pJNK levels as well as fibroblast apoptosis were almost completely blocked (Fig. 7, D-F). Hence, both in vitro and in vivo, *Mmp14* maintains dermal fibroblast survival by actively suppressing a pJNK-dependent pathway that is triggered when collagen matrix remodeling is ablated.

Discussion

By E18.5, dermal fibroblasts have differentiated into papillary and reticular populations, a point in time during which the ECM remains immature (Driskell and Watt, 2015; Rognoni and Watt, 2018; Smith et al., 1982). During the following early postnatal period, dermal fibroblasts begin synthesizing and depositing a complex network of covalently crosslinked type I collagen, eventually comprising ~70% of the dermal ECM (Smith et al., 1982). Consistent with earlier work documenting the selective degradation of skin collagen during the rapid phases of postnatal growth (Klein and ChandraRajan, 1977), we find that *Mmp14* is expressed throughout the dermal compartment in association with the appearance of degraded type I collagen during this timeframe. In turn, *Mmp14*-dependent matrix remodeling regulates mechanotransduction cascades critical to fibroblast survival. As an important aside, it should be noted that dermal type I collagen fibrils are normally decorated with type III collagen (Keene et al., 1987), potentially complicating the collagenolytic process. Nevertheless, *Mmp14* can hydrolyze type III collagen (Ohuchi et al., 1997) with more recent reports indicating that the type III collagen content of mouse skin is low in the early postnatal period (Arai et al., 2017).

The observed increases in fibroblast apoptosis found in the dermis of *Mmp14*^{-/-} mice are likely pathognomonic of distinct derangements occurring throughout the tissues of these animals, with specific effects exerted as a function of the distinct characteristics of the various cell types and organ systems (Chan et al., 2012; Chun et al., 2006; Feinberg et al., 2018; Gonzalo et al., 2010; Jin et al., 2011; Tang et al., 2013). For example, *Mmp14*-targeted mesenchymal stem cells do not undergo apoptosis in vivo but instead alter lineage commitment programs from

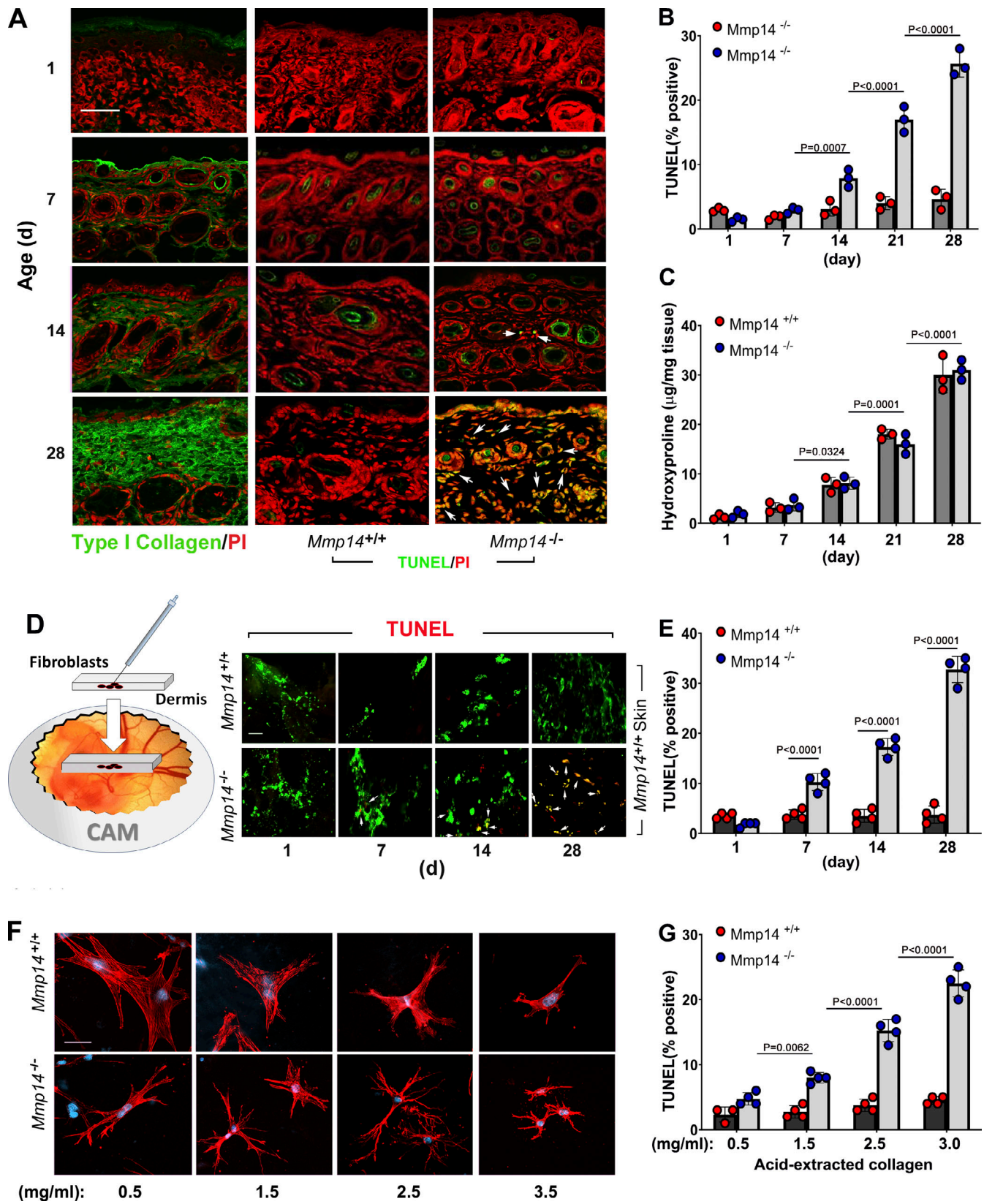


Figure 4. **Postnatal maturation of the dermal extracellular matrix. (A and B)** (A) Dorsal skin was harvested from 1-, 7-, 14-, and 28-day-old *Mmp14*^{+/+} or *Mmp14*^{-/-} mice, and type I collagen was visualized by immunofluorescence (with PI counterstaining) and apoptotic cells were detected as TUNEL-positive cells (bar = 50 µm). Results are representative of three independent experiments performed. In panel B, results are quantified as the percentage of positive cells in 10 random fields of tissue sections isolated from three mice (mean ± SEM; n = 3 independent experiments) with P values determined by two-way ANOVA and Tukey post-test. **(C)** Collagen levels were quantified by hydroxyproline assay (mean ± SEM; n = 3) with P values determined by two-way ANOVA and Tukey

post-test. **(D)** The left panel is a schematic of the injection of wild-type or *Mmp14* knockout dermal fibroblasts injected into wild-type skin explants and cultured atop the chick chorioallantoic membrane (CAM). In the panel to the right, *Mmp14^{+/+}* or *Mmp14^{-/-}* dermal fibroblasts (labeled with green microspheres) were injected into normal skin explants harvested from 1-, 7-, 14-, and 28-day-old wild-type mice and cultured atop the chorioallantoic membrane of live chick embryos for 5 days. TUNEL-positive cells in explant cross-sections (red) are marked by white arrows (bar = 20 μ m). **(E)** Number of TUNEL-positive cells as quantified in high power fields taken from 10 randomly selected sections. Results are expressed as the mean \pm SEM ($n = 4$ independent experiments) with P values determined by two-way ANOVA and Tukey post-test. **(F and G)** *Mmp14^{+/+}* or *Mmp14^{-/-}* fibroblasts were embedded in increasingly dense type I collagen hydrogels (0.5–3.5 mg/ml) and stained for F-actin (bar = 100 μ m) (F) or TUNEL-positive cells (G). Results are expressed as the mean \pm SEM ($n = 4$ independent experiments) with P values determined by two-way ANOVA and Tukey post-test.

osteoblastogenesis to adipogenesis and chondrogenesis (Tang et al., 2013, 2022). Further, the striking sensitivity of dermal fibroblasts to *Mmp14*-regulated cell survival does not extend to *Mmp14^{-/-}* cardiac, lung, or mammary fibroblasts where 3-D survival remains unaffected (Feinberg et al., 2018; Koenig et al., 2012; Rowe et al., 2011). These results most likely reflect the functional heterogeneity displayed by mesenchymal cell populations residing in different host microenvironments as well as their *Mmp14*-specific requirements (Buechler et al., 2021; Chang et al., 2002; Driskell and Watt, 2015; Rinn et al., 2006). We do note, however, that an earlier report described increased osteocyte apoptosis in *Mmp14^{-/-}* mice (Karsdal et al., 2004), but later studies failed to confirm this observation in vivo (Holmbeck et al., 2005). Likewise, while *Mmp14* has been reported to regulate the expression of *BIK*, a proapoptotic tumor suppressor in cancer cells (Maquoi et al., 2012), we detected no changes in its expression in *Mmp14*-null fibroblasts nor were increases in apoptosis observed in *Mmp14*-null carcinomas in vivo (Feinberg et al., 2018). Taken together, we conclude that *Mmp14* acts as a required, prosurvival factor in developing dermal tissues in the early postnatal period.

Given the morbidity and accelerated mortality of *Mmp14^{-/-}* mice (Holmbeck et al., 1999; Zhou et al., 2000) and the impact of global knockout on multiple systems, ranging from adipogenesis to branching morphogenesis (Alabi et al., 2021; Chan et al., 2012; Chun et al., 2006; Feinberg et al., 2018; Gonzalo et al., 2010; Jin et al., 2011; Shimizu-Hirota et al., 2012; Tang et al., 2013), we considered the possibility that dermal fibroblast apoptosis might not reflect a cell-autonomous defect in vivo. However, the cell death phenotype is readily recapitulated in vitro when *Mmp14*-null fibroblasts are embedded in 3-D hydrogels designed to recreate the ECM of type I collagen-rich dermal tissues. With the limited life span of *Mmp14* global knockout mice (in our studies, targeted mice live no longer than 6 wk), the long-term functional impact of *Mmp14* targeting on dermal fibroblast function will require the use of conditional knockouts. However, such studies are complicated by the fact that other dermal cell populations, including preadipocytes, adipocytes, endothelial cells, smooth muscle cells, and pericytes, likewise express *Mmp14* and potentially participate in dermal collagenolysis in a compensatory fashion (Chun et al., 2004; Filippov et al., 2005; Lehti et al., 2005; Yana et al., 2007). Furthermore, *Mmp14* is readily shed in exosomes, thereby allowing transcellular import into targeted cell populations in vivo (Crewe et al., 2018; Shimoda and Khokha, 2017). Interestingly, in recent work, *Mmp14* was targeted in fibroblasts in vivo, resulting in dermal fibrosis, but apoptosis was not examined (Zigrino et al., 2016). However, in these conditional knockout mice, targeting was initiated at P30

(Zigrino et al., 2016), a time point at which the bulk of dermal collagen remodeling is complete. In this regard, *Mmp14* global knockout mice display more severe phenotypes relative to conditional knockout mice when global targeting is initiated in adult mice (Xia et al., 2023).

In considering the potential mechanisms by which *Mmp14* functions to maintain fibroblast viability, efforts to gain mechanistic insights are complicated by the fact that the proteinase is able to cleave a large number of membrane-associated targets, ranging from integrins and syndecans to membrane-anchored growth factors and receptors (Itoh, 2015; Rowe and Weiss, 2009). Nevertheless, *Mmp14^{-/-}* fibroblast viability is maintained when cultured either under standard 2D culture conditions or atop collagen hydrogels, effectively ruling out a requirement for the shedding or activation of cell surface or secreted molecules—at least under these culture conditions. Alternatively, type I collagen hydrogels have been reported to modulate cell function in 3-D culture by regulating either integrin- or non-integrin-dependent signaling (Birukawa et al., 2014; Koyama et al., 1996; Montgomery et al., 1994; Wall et al., 2007; Zhou et al., 2006). However, when 3-D collagen hydrogels are assembled under conditions where lysyl oxidase-derived aldimine crosslinks cannot form (Sabeh et al., 2009b), we find that *Mmp14* is no longer required to maintain the viability of embedded fibroblasts. Hence, it is the mechanical—rather than structural—properties of the collagen hydrogel that serve as the most important determinant of fibroblast responses. Though recent studies have reported no differences in fibroblast behavior when suspended in native versus non-crosslinked collagen hydrogels (Lakshman and Petroll, 2012; Zhou and Petroll, 2014), a functional role for MMPs in regulating cell survival is clearly restricted to the native, crosslinked material. Further, our studies with PEG-based synthetic hydrogels highlight the fact that proteolysis of native, crosslinked type I collagen per se is not required for maintaining fibroblast survival, thereby ruling out the possibility that collagen degradation itself plays a required role in this system. Rather, the key signal to maintaining fibroblast survival is directly linked to protease-dependent regulation of 3-D cell shape, contractility, and mechanotransduction-linked signaling. Interestingly, we attempted to extend these studies to include the use of collagenase-resistant type I collagen isolated from *Coll1^{r/r}* mice (Liu et al., 1995), which would be predicted to induce cell death in wild-type fibroblasts. To our surprise, we have found that wild-type fibroblasts are able to degrade r/r collagen by a heretofore undescribed mechanism that requires both *Mmp14* and a TIMP-1-sensitive, secreted MMP (Fig. S6). While these findings preclude the use of r/r collagen in our studies, all of the findings reported herein remain consistent with

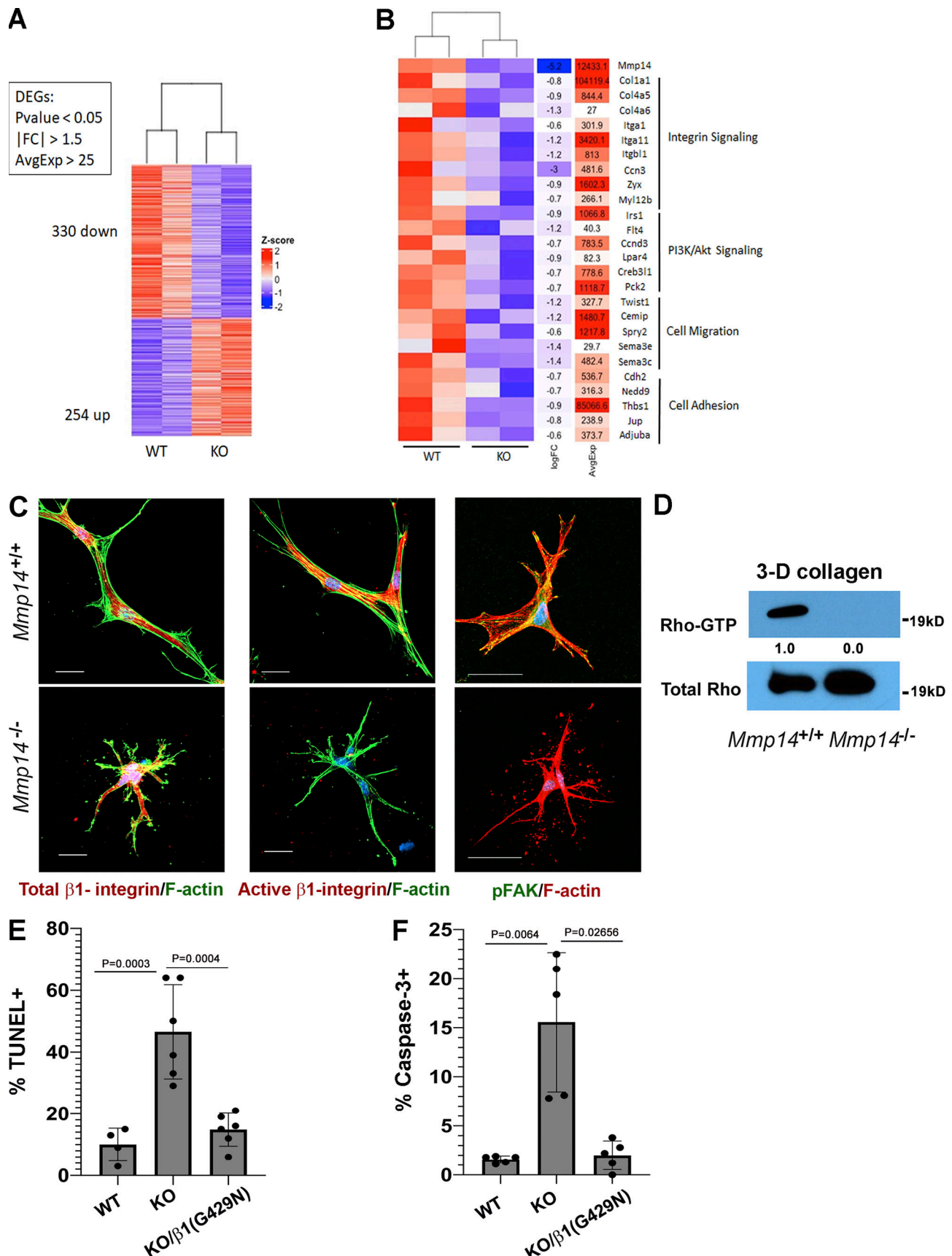


Figure 5. **Transcriptional profiling and functional analyses identify defects in β 1 integrin signaling in *Mmp14*^{-/-} fibroblasts.** (A) Heatmap displaying a scaled expression of differentially expressed genes (DEGs; P value <0.05; fold change [FC] > 1.5 or less-than -1.5; average expression >25 counts) between

wild-type (WT) and *Mmp14* knockout (KO) fibroblasts embedded in 3D type I collagen for 48 h. **(B)** Heatmap displaying differentially expressed genes grouped by pathways identified as downregulated in *Mmp14*-null fibroblasts via pathway analysis of Gene Ontology biological processes and Kyoto Encyclopedia of Genes and Genomes pathway gene sets. **(C)** *Mmp14*^{+/+} or *Mmp14*^{-/-} fibroblasts were embedded in type I collagen hydrogels, and after a 36-h culture period, stained for total β 1 integrin, activated β 1 integrin (bar = 25 μ m), or pFAK and F-actin (bar = 50 μ m). Results are representative of three or more experiments. **(D)** Rho-GTP levels were determined by immunocapture and western blot (results representative of two independent experiments performed). Relative expression levels are shown as determined by densitometry. **(E and F)** Wild-type (WT), *Mmp14* knockout (KO) cells, or *Mmp14* KO cells were transduced with a constitutively active G429N β 1 integrin mutant, embedded in 3-D collagen hydrogels for 120 h, and the percent TUNEL-positive and caspase-3-positive cells determined. Data are presented as mean \pm SEM ($n = 6$ independent experiments) with P values determined by one-way ANOVA and Tukey post-test. Source data are available for this figure: SourceData F5.

the conclusion that pericellular proteolysis of native or synthetic matrices is central to the activation of a mechanotransduction-linked cell survival program.

Given a requirement for the activation of *Mmp14*-dependent signaling cascades to maintain dermal fibroblast survival, it has been perplexing that newborn *Mmp14*^{-/-} mice appear largely indistinguishable from littermate controls, but embryonic tissues in the developing mouse—save for the vasculature and bone—contain only low levels of type I collagen (Feinberg et al., 2016; Holmbeck et al., 1999; Lohler et al., 1984; Tang et al., 2013; Zhou et al., 2000). Apparently, the most dramatic increases in dermal type I collagen levels are reserved for early postnatal development, likely as a means to accommodate the mechanical stresses associated with the ex utero environment. As such, and as highlighted here in our analyses of dermal tissues, *Mmp14*^{-/-}-associated pathology displays itself as a function of the deposition of a mechanically mature ECM (Fig. 8).

During wound healing, fibroblasts proliferate and purposefully increase cytoskeletal tension and tractional forces in an effort to draw the edges of the damaged tissue together (Darby et al., 2002; Kobayashi et al., 2005; Nho et al., 2005; Niland et al., 2001). At the close of this process, tractional forces are no longer required and the wound fibroblasts transition from a “stressed” to a “relaxed” state that triggers a wave of apoptosis to restore fibroblast numbers to their prewound state (Darby et al., 2002; Kobayashi et al., 2005; Nho et al., 2005; Niland et al., 2001). Early studies have demonstrated that this program can be recapitulated in vitro (Kobayashi et al., 2005; Nho et al., 2005; Niland et al., 2001). That is, when fibroblasts are embedded in collagen hydrogels that remain adherent to the surrounding walls of culture dishes, the elongating cells increase cytoskeletal tension and the rigidity of the cell-hydrogel composite increases with the system classified as mechanically stressed. If the gel is then detached from the walls of the culture dish, the embedded fibroblasts contract the gel, and the change in cell shape and mechanical rigidity triggers an apoptotic response similar to that observed during wound closure in vivo (Kobayashi et al., 2005; Nho et al., 2005; Niland et al., 2001). Interestingly, this tension/relaxation-induced form of apoptosis has previously been associated with increased TGF- β levels both in vitro and in vivo (Bouffard et al., 2008; Maeda et al., 2011; Varedi et al., 2000). Though active TGF- β can exert myriad effects on cell function via canonical and non-canonical signaling pathways (Massague, 2012), cellular responses are tightly linked to ECM rigidity with cell death triggered as the malleability of the underlying matrix increases (Leight et al., 2012). Indeed, recent studies indicate that disruption of cellular tension drives the reorganization of TGF- β receptors, thereby

allowing Smad activation (Rys et al., 2015). Apparently, *Mmp14*^{-/-} fibroblasts appear to “read” their inability to adopt normal cell shapes and increase pericellular matrix rigidity as a signal to downregulate β 1 integrin signaling and engage a TGF- β -induced cell death program similar to that observed during wound healing. While the effects of deleting *Mmp14* expression in 3-D-embedded fibroblasts are complex, highlighting the existence of a mechanically coupled system, a critical role for β 1 integrin activation is highlighted by the ability of a constitutively active integrin mutant to maintain the viability of *Mmp14* knockout fibroblasts despite the continued absence of collagenolytic activity. A TGF- β /JNK cascade has not been previously linked to dermal fibroblast apoptosis, but TGF- β triggers stress-induced JNK-mediated apoptosis in other cell systems (Lee and Schiemann, 2011; Lei et al., 2002; Schuster et al., 2002; Wang et al., 2007). Interestingly, we find that the apoptosis program activated in *Mmp14*^{-/-} fibroblasts can be duplicated when normal fibroblasts are embedded within relaxed hydrogels (Fig. S5, F and G). Further studies are nevertheless needed to characterize the mechanisms underlying increased TGF- β expression and activation in *Mmp14*-null fibroblasts as well as wild-type fibroblasts cultured in relaxed gels (Fig. S5 F).

Taken together, our data demonstrate that wild-type fibroblasts purposefully mobilize *Mmp14* during the early postnatal changes associated with the development of the dermal ECM in a concerted effort to optimally maintain cell shape, cytoskeletal tension, and β 1 integrin-linked mechanotransduction. In the absence of *Mmp14*, fibroblasts are unable to properly adjust their interactions with the surrounding ECM, thereby creating a scenario in which the cells inappropriately engage an apoptotic program that we postulate recapitulates that activated during wound healing (Fig. 8). As such, the *Mmp14*-dependent remodeling of the collagenous matrix can now be classified as a new prosurvival axis whose proteolytic activity is required to maintain dermal fibroblast function. Given the fact that matrix-degradative activity of *Mmp14*, whether expressed by fibroblasts or other dermal cell populations, can regulate tissue-invasive activity through both normal and provisional matrices (Hotary et al., 2002; Rowe et al., 2011; Sabe et al., 2009a), proliferative responses as well as normal tissue homeostasis (Zigrino et al., 2016), it seems likely that this proteinase will play more global roles in regulating dermal function in health and disease, not only in mice but humans as well.

Materials and methods

Mice

Mmp14^{+/+} mice (outbred Swiss Black background), *Mmp14*^{+/LacZ} mice (C57BL/6 background), and *Mmp14*^{ff/ff} mice (outbred Swiss

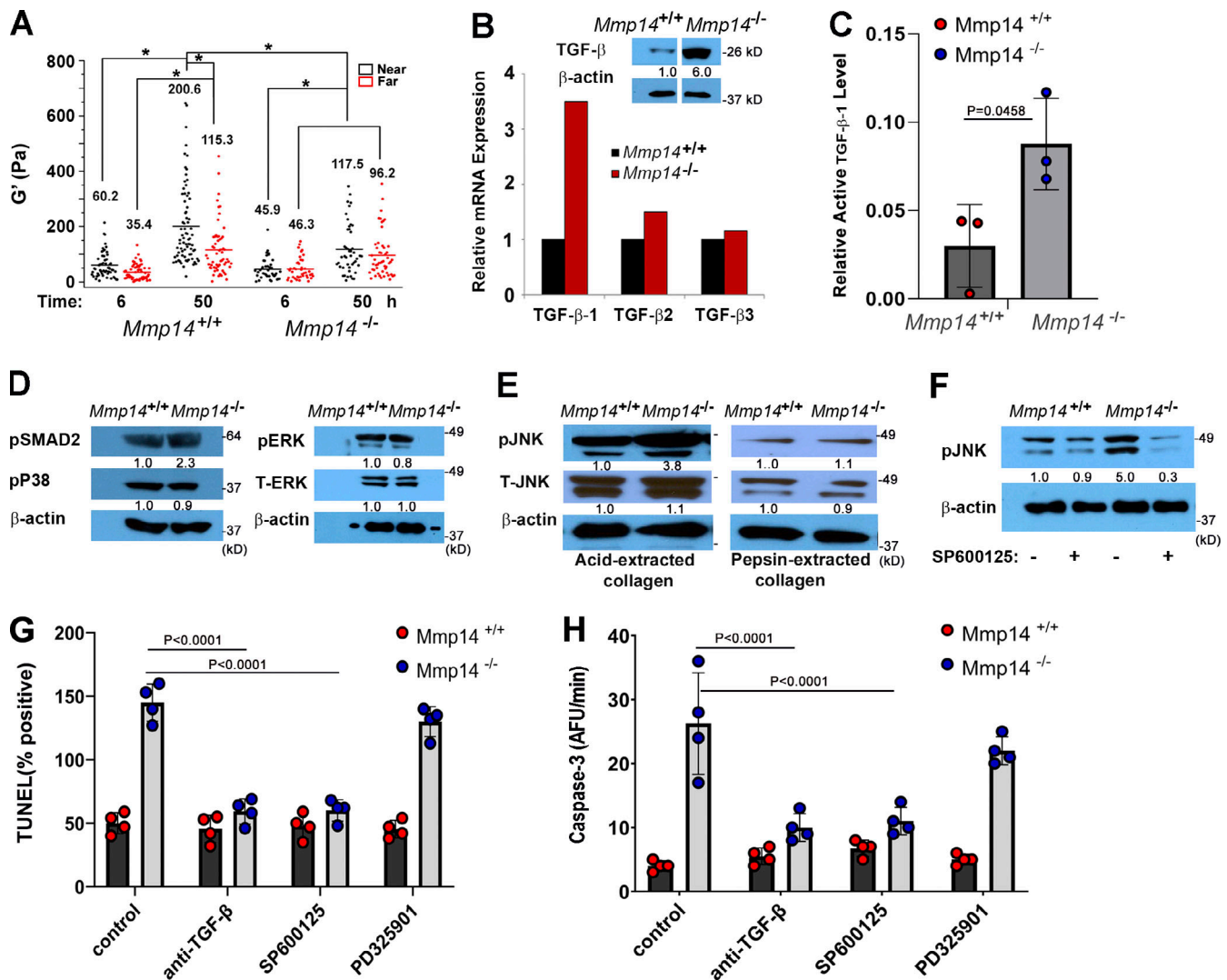


Figure 6. A TGF- β /JNK cascade induces fibroblast apoptosis. (A) *Mmp14*^{+/+} or *Mmp14*^{-/-} fibroblasts were embedded in type I collagen hydrogels, and the pericellular rigidity of the matrices was monitored by optical tweezer-based active microrheology either near (<5 μ m) or distant (>100 μ m) from the fibroblasts. Elastic modulus values (G') of beads at 6 and 50 h are shown. Each point represents the average G' (across frequencies) for each bead. Results are presented as mean \pm SEM, * P < 0.05; two-way ANOVA and Tukey post test. (B and C) Relative mRNA levels of TGF- β isoforms (B), TGF- β protein levels (B inset), and active TGF- β 1 levels (C) expressed in *Mmp14*^{+/+} or *Mmp14*^{-/-} fibroblasts embedded in 3-D type I collagen hydrogels for 24 h. Results are representative of two independent experiments performed in panel B and three independent experiments with mean \pm SEM as assessed by Student's t test in panel C. Relative expression levels for western blot (B) are shown as determined by densitometry. (D) Western blot of pSMAD2, p-p38, pERK, and total ERK (T-ERK) levels in *Mmp14*^{+/+} or *Mmp14*^{-/-} fibroblasts cultured in 3-D collagen for 24 h (results representative of three independent experiments performed). Relative expression levels for western blots are shown as determined by densitometry. (E) pJNK1,2 and total JNK1,2 (T-JNK) levels in *Mmp14*^{+/+} versus *Mmp14*^{-/-} fibroblasts embedded in 3-D native or pepsin-extracted collagen hydrogels for 24 h as determined by western blot analysis. Relative expression levels for western blots are shown as determined by densitometry. Results are representative of three independent experiments performed. (F) pJNK levels in *Mmp14*^{+/+} or *Mmp14*^{-/-} fibroblasts embedded in 3-D type I collagen hydrogels in the absence or presence of the JNK inhibitor, SP600125, for 24 h as determined by western blot. Relative expression levels for western blots are shown as determined by densitometry. Results are representative of three independent experiments performed. (G and H) *Mmp14*^{+/+} or *Mmp14*^{-/-} fibroblasts were cultured in native, 3-D collagen hydrogels in the absence or presence of either anti-TGF- β antibodies, the MEK inhibitor, PD325901, or SP600125 for 5 days and TUNEL-positive cells (G) and caspase-3 activity (H) quantified. Results are expressed as a mean \pm SEM (n = 4 independent experiments) with P values determined by two-way ANOVA and Turkey post-test. AFU, active fluorescent units. Source data are available for this figure: SourceData F6.

Black background) were generated as described previously (Holmbeck et al., 1999; Tang et al., 2013; Yana et al., 2007).

Isolation and culture of mouse dermal fibroblasts

Fibroblasts were isolated from dorsal dermal explants or collagenase digests of 2–7-day-old wild-type mice, mutant, or littermate controls (Driskell and Watt, 2015; Driskell et al., 2013;

Sabeh et al., 2004). In selected experiments, papillary and reticular dermal fibroblasts recovered from collagenase digests were sorted by flow cytometry using antibodies directed against Lrig1 (FAB3688G, Goat; R&D), Sca-1 (AF1226, Goat; R&D), integrin- α 8 (AF4076, Goat; R&D), and Dlk1 (MAB8634, Rabbit; R&D) (Driskell et al., 2013). Fibroblasts (used between passages 2–6) were cultured in DMEM supplemented with 10% heat-inactivated fetal calf serum

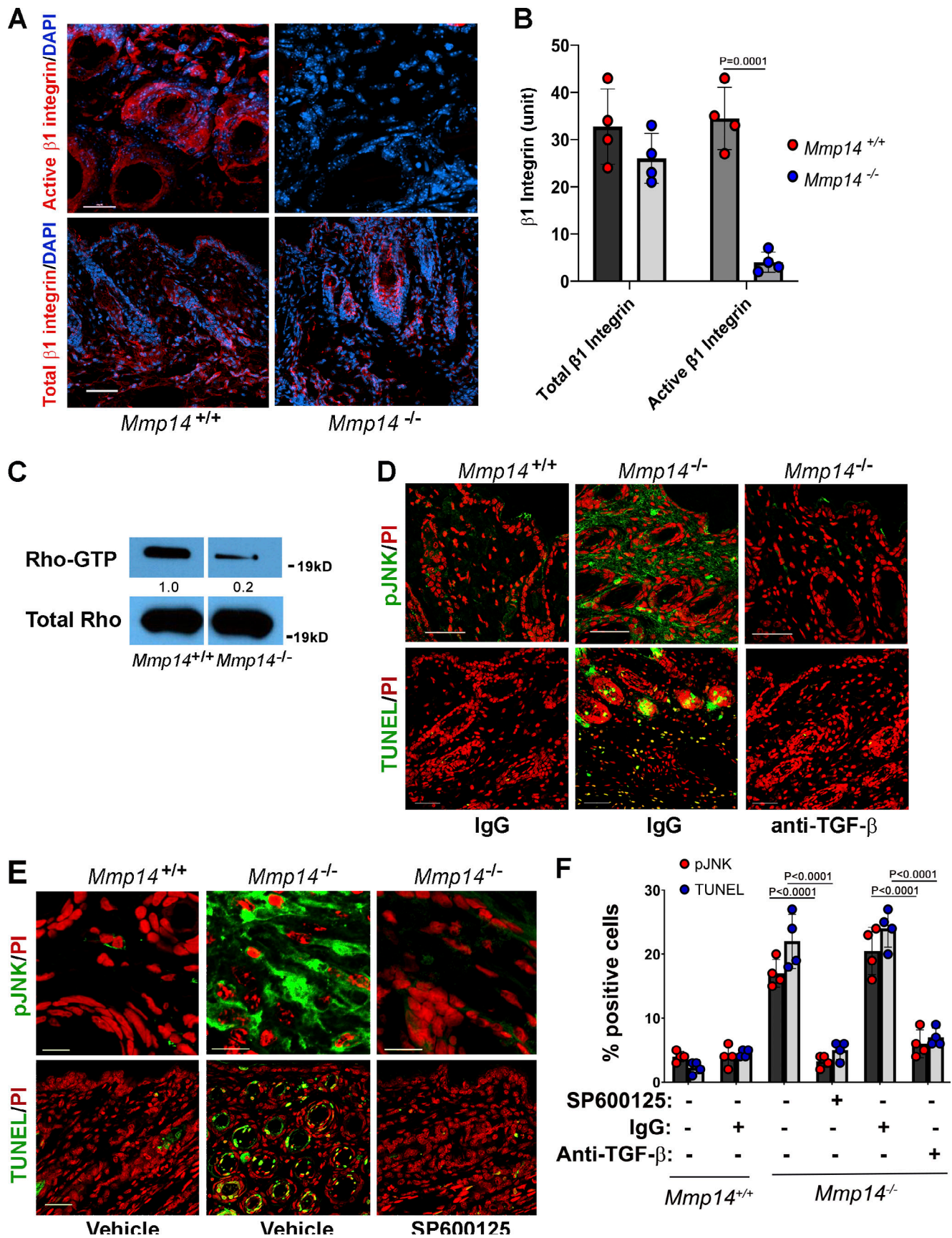


Figure 7. **A** TGF- β /JNK axis regulates *Mmp14*^{-/-} dermal apoptosis in vivo. **(A and B)** Active and total $\beta 1$ integrin expression in skin cross-sections of 3-wk-old wild-type versus *Mmp14*-null mice as assessed by immunofluorescence in panel A (red; bar = 50 μ m) and following quantitative image analysis (B). Results

are expressed as the mean \pm SEM; $n = 4$ independent experiments as assessed by Student's *t* test. **(C)** Western blot of Rho-GTP levels in skin extract of 3-wk-old wild-type versus *Mmp14*-null mice. Relative expression levels for western blots are shown as determined by densitometry. Results representative of two independent experiments performed. **(D and E)** pJNK and TUNEL in cross-sections of dorsal skin excised from 3-wk-old wild-type versus *Mmp14*-null mice treated with either IgG or anti-TGF- β neutralizing antibody (D; all bars = 50 μ m) or SP600125 for 3 wk (E; pJNK, bars = 5 μ m and TUNEL, bars = 50 μ m). Data are representative of two independent experiments performed, each with $n = 3$ mice. **(F)** Quantification of pJNK- and TUNEL-positive cells from C and D ($n = 3$ independent experiments). Data are presented as mean \pm SEM ($n = 4$ independent experiments) with *P* values determined by two-way ANOVA and Turkey post-test. Source data are available for this figure: SourceData F7.

(FCS; Atlanta Biologicals) or heat-inactivated mouse sera, 100 U/ml penicillin, 100 μ g/ml streptomycin, 0.25 μ g/ml fungizone, and 2 mM *L*-glutamine.

Fibroblast-collagen composites

Type I collagen was acid- or pepsin-extracted from rat tail tendons (Sabeh et al., 2009a) while pepsin-extracted bovine dermal collagen was obtained commercially (Vitrogen; Nutacon). Reduced rat tail collagen was prepared via sodium borohydride reduction (Gelman et al., 1979; Sabeh et al., 2009a). Collagen rigidity was determined in an RSFII rheometer (Rheometrics) using dynamic shear mode and parallel plates in a hydrated chamber while pore size was approximated by confocal reflection microscopy (Dudley et al., 2014; Wolf et al., 2013). Fibroblasts (5×10^4) were either cultured atop or embedded within collagen hydrogels (0.5–3.5 mg/ml with 2.2 mg/ml used as the standard concentration) (Sabeh et al., 2004). For PEG-

based, RGD-derivatized hydrogel cultures, the cells were mixed with hydrogel solution and cultured according to the manufacturer's protocol (QGel SA; QGel Bio) (Tang et al., 2013).

In all experiments, fibroblast-hydrogel cultures were performed in 10% heat-inactivated FCS alone or with the recombinant MMP inhibitor, TIMP-2 (3 μ g/ml; Fuji Industries), TGF- β 1 (10 ng/ml; R&D Systems), TGF- β neutralizing antibody (1 μ g/ml; AB-100-NA, Rabbit; R&D), the MEK inhibitor, PD325901 (10 nM; LC Laboratories), the JNK inhibitor, SP600125 (20 μ M; Sigma-Aldrich), or Benzyl-oxy-carbonyl-Val-Ala-Asp(OMe)-fluoromethylketone (*Z*-VAD) (10 μ M; R&D Systems).

Lentiviral transduction

Mmp14-null fibroblasts were transduced with full-length MMP14, catalytically inactive MMP14, MMP14 deletion mutants, MMP14/MMP1 chimeric constructs, or a constitutively active G429N

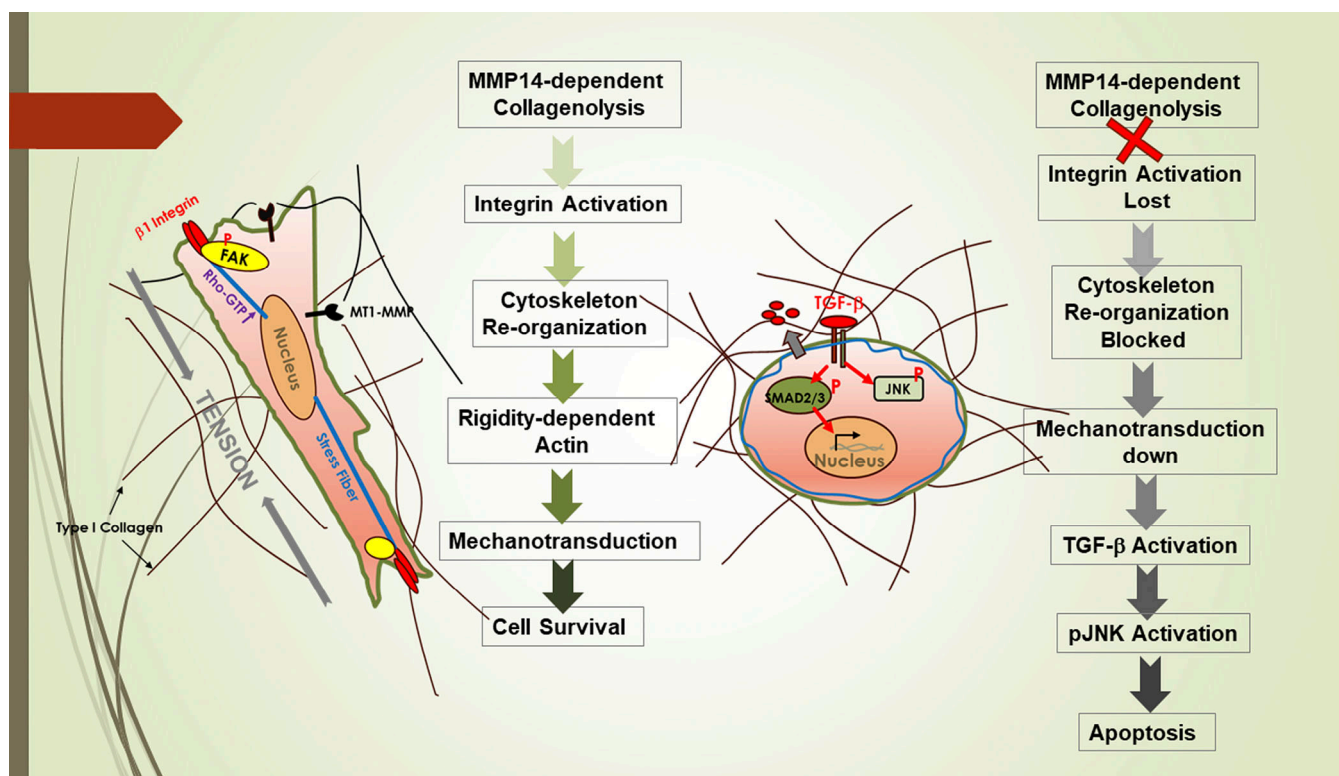


Figure 8. **Schematic overview of the *Mmp14* dermal fibroblast survival program.** During early postnatal development of the dermis, type I collagen-embedded fibroblasts undergo shape changes driven by *Mmp14*-dependent pericellular proteolysis of the surrounding matrix that coincidentally triggers β 1 integrin activation, thereby setting in motion a cascade of mechanotransduction-linked events, including increased pFAK and Rho-GTP kinase levels, and increased cytoskeletal tension as well as matrix rigidity that together maintain cell survival. By contrast, in the absence of *Mmp14*-dependent pericellular collagenolysis, dermal fibroblasts are encased in a matrix that limits cell spreading and all of the associated mechanotransduction-linked steps, resulting in the loss of cytoskeletal tension and an inability to increase ECM rigidity. Via unknown mechanisms similar to those observed in wound healing, the absence of cell-matrix tension triggers an increase in TGF- β expression and activation that then actuates a pJNK-dependent apoptotic program.

$\beta 1$ integrin mutant with all constructs cloned into a lentiviral expression vector (Li et al., 2008; Sabeh et al., 2009b). The expression levels and collagenolytic activity of endogenous Mmp14 versus MMP14 as well as MMP14 mutant constructs are shown in Fig. S7.

Quantitative polymerase chain reaction (qPCR)

Total RNA was extracted using a TRIzol kit and cDNA was synthesized using the Superscript III kit (Invitrogen Life Technologies). qPCR was performed using SYBR-Green Supermix (Invitrogen Life Technologies). Mouse TGF- $\beta 1$ primers; forward: 5'-TGATACGCCTGAGTGGCTGTCT-3', reverse: 5'-CACAAAGAGCAGTGAGCGCTGAA-3'. Mouse TGF- $\beta 2$ primers; forward: 5'-CCG CATCTCCTGCTAATGTTG-3', reverse: 5'-AATAGCGGCATCCA AAGC-3'. Mouse TGF- $\beta 3$ primers; forward: 5'-AAGCAGCGCTAC ATAGGTGGCA-3', reverse: 5'-GGCTGAAAGGTGTGACATGGAC-3'. Mouse GAPDH primers; forward: 5'-CATCACTGCCACCCA GAAGACTG-3', reverse: 5'-ATGCCAGTGAGCTTCCCGTTCAG-3'.

Western blotting and ELISA

Cells in either 2-D or 3-D culture or skin tissue were homogenized and lysed with radioimmunoprecipitation assay buffer, and the lysate (20–30 μ g) was boiled with or without reducing agent (for TGF- β analyses) and resolved by 4–20% SDS-polyacrylamide gel electrophoresis followed by blotting onto polyvinylidene fluoride membranes (Bio-Rad Laboratories). For analyses of lamin A/C content, the cells were lysed in Laemmli buffer (Bio-Rad). Antibodies for western blots include anti-Mmp14 (#2010-1, Rabbit; Epitomics), hemagglutinin (HA, HA.C5; ab18181, Mouse; Abcam), anti-lamin A/C (sc-376248, Mouse; Santa Cruz Biotechnology), anti-p21 (ab188224, Rabbit; Abcam), anti-glyceraldehyde-3-phosphate dehydrogenase (CB1001, Mouse; Sigma-Aldrich), pan anti-TGF- β (AB-100-NA, Rabbit; R&D), anti-pP38 (#4511, Rabbit; Cell Signaling) and total P38 (#9212, Rabbit; Cell Signaling), anti-pJNK1,2 (#9251, Rabbit; Cell Signaling) and total JNK1,2 (#9252, Rabbit; Cell Signaling), anti-pERK (#4377, Rabbit; Cell Signaling) and total ERK (#4695, Rabbit; Cell Signaling), anti- γ -H2AX (#9718, Rabbit; Cell Signaling), anti-pFAK (Tyr 397; ab81298, Rabbit; Abcam), anti-pSMAD2 (#3108, Rabbit; Cell Signaling), and anti- β -actin (MAB8929, Mouse; R&D). Secondary antibodies for western blots were Cell Signaling #7076 (HRP-linked, anti-mouse) and Cell Signaling #7074 (HRP-linked, anti-rabbit). Rho and Rho-GTP levels were determined using a Rho activation assay kit (#8820; Cell Signaling). Active TGF- β levels were determined in cell-free supernatants by ELISA (Legend Max Free Active TGF- $\beta 1$ ELISA Kit; Biolegend).

Optical tweezer-based active microrheology analysis of ECM rigidity

Collagen gels containing skin fibroblasts and 2 μ m carboxylated beads (Bangs Laboratories) were polymerized within glass-bottom Petri dishes. After a 6- or 50-h incubation period, the microrheology system was performed (Kotlarchyk et al., 2011; Tang et al., 2013). Briefly, a focused laser-trapping beam (1,064 nm) oscillates transversely about the center of a bead with an amplitude of 60 nm at a set of oscillation frequencies (10, 20, 30, and 50 Hz). As the laser pulls the bead away from equilibrium,

elastic forces of the ECM act to restore it. A stationary detection laser (785 nm) was used to track the bead position in time on a Quadrant Photo Detector while a Position Sensing Detector was used to track the position of the trapping laser. From these signals, a complex shear modulus (G^*) is computed that comprises real (G') and imaginary (G'') components, where G' is the elastic modulus. Measurements were conducted near (within 5 μ m) and far (>100 μ m) from both *Mmp14*^{+/+} and *Mmp14*^{-/-} fibroblasts.

Dermal collagen content

The collagen content of skin explants was quantified by hydroxyproline assay in acid (6N HCl) hydrolysates (Creemers et al., 1997; Sabeh et al., 2004).

Histology, immunofluorescence, apoptosis/senescence assays, and EM

Skin, lung, tail, or brain from 1-day- to 1-mo-old mice were dissected, fixed in 4% paraformaldehyde, frozen or embedded in paraffin, and sectioned (5–10 μ m). Sections were stained with Hematoxylin/Eosin (H&E) or Trichrome according to standard procedures (Tang et al., 2013). LacZ activity was analyzed in frozen sections (Tang et al., 2013). H&E, LacZ, and Trichrome images were acquired with an Olympus BX51 upright microscope (Olympus; 10 \times , 20 \times , or 40 \times objectives/0.4, 0.7, or 0.9 NA, respectively) and digitally acquired using a DP70 digital camera at 25°C.

Immunofluorescence was performed on frozen sections of mouse tissues (skin, tail, lung, heart, and brain) or in fibroblast-collagen cultures following fixation in 1–4% paraformaldehyde. Type I collagen content was assessed in tissue sections by either staining with anti-type I collagen polyclonal antibodies (AB765P, Rabbit; Sigma-Aldrich), assessing second harmonic generation in frozen sections (Morishige et al., 2006; Tang et al., 2013), or by Trichrome staining paraffin sections. Immunofluorescent staining of denatured collagen in frozen sections of skin or collagen hydrogels was determined with anti-Coll-1/3/4C polyclonal antibody (#0217-050, Rabbit; ImmunoGlobe) (Tang et al., 2013). Apoptosis was assessed in fibroblast cultures or tissue sections using a TUNEL assay kit (Click-iT Plus TUNEL assay; Life Technologies, or TdT In Situ Apoptosis Detection kit; R&D Systems). For in vivo detection of senescent cells, cross-sections of frozen tissue were prepared, and β -galactosidase activity at pH 6.0 was detected according to the manufacturer's instruction (Senescence β -Galactosidase Staining kit; Cell Signaling). Active caspase-3 levels in fibroblast cultures were determined using an active caspase staining kit (CaspGLOW; Biosource) and a fluorescent plate reader. Total and active $\beta 1$ integrins were detected using anti- $\beta 1$ integrin antibody (clone MB1.2, MAB11997, Rat; Millipore) and anti-active $\beta 1$ integrin antibody (clone 9EG7, 550531, Rabbit; BD Biosciences), respectively. To quantify corrected total cellular fluorescence, the channel detecting nuclear DAPI staining was first used to identify cellular regions of each image to be used for quantification. Next, fluorescent signal from the specified antibody was quantified in those regions, normalizing for background signal detected in nearby acellular regions. Last, total fluorescent intensity measured in cellular regions was further normalized by dividing the total fluorescent

intensity by the total area of the cellular region defined for that image as outlined (Shihan et al., 2021).

Fibroblast morphology in vitro was assessed using a laser-scanning confocal microscope (Nikon A1/A1R inverted microscope) using either 40× or 60× C-Apochromat (1.2 NA) water immersion objectives at 25°C. Samples were mounted in fluorescent mounting media (DakoCytomation) and stained with either Alexa Fluor 488 (green) or Alexa Fluor 594 (red) phalloidin, and either propidium iodide (PI) or DAPI (Invitrogen). All fluorescence images were analyzed with Adobe Photoshop (CS6). Transmission and scanning electron microscopy were performed and imaged with a JEOL JEM-1400 Plus electron microscope or AMRAY 1910 Field Emission Scanning Electron Microscope. Images were recorded using a Hamamatsu ORCA-HR digital camera system and ATM software (Advanced Microscopy Techniques Corporation) (Chun et al., 2006; Sabeh et al., 2009b).

Secondary antibodies used for immunostaining include Alexa Fluor 488 (A11034, Anti-rabbit; Invitrogen), Alexa Fluor 594 (A11012, Anti-rabbit; Invitrogen), Alex Fluor 488 (A11001, Anti-mouse; Invitrogen), and Alexa Fluor 594 (A11005, Anti-mouse; Invitrogen).

RNA sequencing (RNA-seq) analysis

Total RNA was extracted using TRIzol. Libraries were then prepared using the NEBNext rRNA Depletion Kit (E6310; NEB) and NEBNext Ultra II Directional RNA Library Prep Kit (E7760; NEB). The libraries were subject to 150 bp paired-end cycles on the NovaSeq-6000 platform (Illumina). Reads were trimmed using Cutadapt v2.3 (Martin, 2011) and then evaluated using FastQC (v0.11.8) (Andrews, 2010) to determine the quality of the data. Reads were mapped to the mm10 reference genome, GRCm38 (ENSEMBL), using STAR (v2.7.8a) (Dobin et al., 2013) and assigned count estimate to genes with RSEM (v1.3.3) (Li and Dewey, 2011). Alignment options followed ENCODE standards for RNA-seq and quality control metrics from several different steps were aggregated by multiQC v1.7 (Ewels et al., 2016). Subsequent analysis of gene expression was performed using the DESeq2 package (v1.42.0) (Love et al., 2014) in R statistical software (v4.3.2). Pathway analysis was performed using DAVID Bioinformatics Resources 2021 (Sherman et al., 2022). Raw and processed data are available at GSE266914.

In vivo inhibition of JNK activation

Mice at 1–4 days of age were administered via intraperitoneal injection (50 µl) of a control IgG or 5 mg/kg TGF-β neutralizing antibody (R&D Systems) every 4 days for a total of three doses. Alternatively, mice received normal saline or SP600125 (Sigma-Aldrich) at a final concentration of 17 mg/kg, every 4 days. Mice were sacrificed at 21 days of age, and skin samples were collected and analyzed for TUNEL staining and JNK activation.

Skin explant culture

Fibroblasts were labeled with fluoresbrite carboxylate microspheres (Polysciences), microinjected (5×10^5 cells) into mouse skin explants collected from 1–28-day-old wild-type mice, and cultured atop the chorioallantoic membrane of 11-day-old chick embryos for 5 days (Sabeh et al., 2009b). The skin explants were

then fixed, frozen sections cut, and examined by TUNEL assay for apoptotic cells.

Mouse type I collagen degradation

Acid-soluble mouse type I collagen was prepared from tail tendons of wild-type or r/r mice (Hotary et al., 2003). Wild-type or Mmp14-null fibroblasts were cultured atop the respective type I collagen hydrogels for 2 days in the absence or presence of 5 µg recombinant TIMP-1 or TIMP-2 (Abcam), and collagen degradation was determined following Coomassie blue staining and destaining (Sabeh et al., 2009a).

Statistical analysis

Results are presented as the mean ± SEM of two or more independent experiments as indicated in the legend of each figure. Data distribution was assumed to be normal, but was not formally tested. The statistical significance threshold was set to a P value of 0.05. P values were determined using a two-tailed Student's *t* test for data with two groups and a one-way analysis of variance (ANOVA) for experiments with more than two groups. Dunnett's test was used to identify differences between a control group and other experimental conditions, while Tukey's honest significance test was employed for other multiple comparisons to obtain corrected P values. In experiments testing the effect or interaction of two independent variables, two-way ANOVA coupled with the relevant post-test was used. The statistical method employed for each experiment is indicated in the corresponding figure legend. GraphPad Prism version 10.2.3 was utilized for analysis.

Online supplemental material

Four supplemental figures and one supplemental table are included, characterizing the Mmp14-dependent control of fibroblast senescence (Fig. S1), the Mmp14-dependent control of fibroblast nuclear structure/damage in 2-D culture (Fig. S2), the Mmp14-dependent regulation of pericellular collagenolysis (Fig. S3), the structural characterization of the dermal extracellular matrix in wild-type versus Mmp14-null mice (Fig. S4), JNK activation and apoptosis in wild-type versus Mmp14 knockout fibroblasts in 2-D versus 3-D culture and in relaxed versus stressed collagen gels (Fig. S5), fibroblast-dependent degradation of wild-type versus r/r collagen (Fig. S6), and the expression and collagenolytic activity of wild-type versus mutant MMP14 constructs in Fig. S7. Mmp expression in wild-type versus Mmp14 knockout fibroblasts in 3-D culture is shown in Table S1.

Data availability

Datasets generated and analyzed in this paper have been deposited to GEO and can be accessed at <https://www.ncbi.nlm.nih.gov/geo/query/acc.cgi?acc=GSE266914>. Any additional datasets or analysis details are available from the corresponding author upon reasonable request.

Acknowledgments

Work performed in this study was supported by grants from the National Institutes of Health, R01-CA-071699-16-A1 (S.J. Weiss),

RO1-HL085339 (E. Botvinick), and P41-EB015890 (E. Botvinick), the Breast Cancer Research Foundation (S.J. Weiss), and Margolies Family Discovery Fund for Cancer Research (S.J. Weiss).

Author contributions: F. Sabeh: Conceptualization, Data curation, Formal analysis, Investigation, Methodology, Project administration, Resources, Software, Supervision, Validation, Visualization, Writing - original draft, Writing - review & editing, X.-Y. Li: Investigation, A.W. Olson: Data curation, Investigation, Writing - review & editing, E. Botvinick: Conceptualization, Formal analysis, Investigation, Methodology, Resources, Visualization, A. Kurup: Data curation, Formal analysis, Investigation, Resources, Visualization, L.E. Gimenez: Formal analysis, Visualization, Writing - review & editing, J.-S. Cho: Investigation, Methodology, Validation, S.J. Weiss: Conceptualization, Data curation, Formal analysis, Funding acquisition, Investigation, Methodology, Project administration, Resources, Supervision, Validation, Visualization, Writing - original draft, Writing - review & editing.

Disclosures: The authors declare no competing interests exist.

Submitted: 18 December 2023

Revised: 10 May 2024

Accepted: 30 May 2024

References

- Alabi, A., X.-D. Xia, H.-M. Gu, F. Wang, S.-J. Deng, N. Yang, A. Adijiang, D.N. Douglas, N.M. Kneteman, Y. Xue, et al. 2021. Membrane type 1 matrix metalloproteinase promotes LDL receptor shedding and accelerates the development of atherosclerosis. *Nat. Commun.* 12:1889. <https://doi.org/10.1038/s41467-021-22167-3>
- Andrews, S. 2010. FastQC: A Quality Control Tool for High Throughput Sequence Data.
- Arai, K.Y., T. Hara, T. Nagatsuka, C. Kudo, S. Tsuchiya, Y. Nomura, and T. Nishiyama. 2017. Postnatal changes and sexual dimorphism in collagen expression in mouse skin. *PLoS One*. 12:e0177534. <https://doi.org/10.1371/journal.pone.0177534>
- Birukawa, N.K., K. Murase, Y. Sato, A. Kosaka, A. Yoneda, H. Nishita, R. Fujita, M. Nishimura, T. Ninomiya, K. Kajiwara, et al. 2014. Activated hepatic stellate cells are dependent on self-collagen, cleaved by membrane type 1 matrix metalloproteinase for their growth. *J. Biol. Chem.* 289:20209–20221. <https://doi.org/10.1074/jbc.M113.544494>
- Bouffard, N.A., K.R. Cutroneo, G.J. Badger, S.L. White, T.R. Buttolph, H.P. Ehrlich, D. Stevens-Tuttle, and H.M. Langevin. 2008. Tissue stretch decreases soluble TGF-beta1 and type-1 procollagen in mouse subcutaneous connective tissue: Evidence from ex vivo and in vivo models. *J. Cell. Physiol.* 214:389–395. <https://doi.org/10.1002/jcp.21209>
- Buechler, M.B., R.N. Pradhan, A.T. Krishnamurthy, C. Cox, A.K. Calviello, A.W. Wang, Y.A. Yang, L. Tam, R. Caothien, M. Roose-Girma, et al. 2021. Cross-tissue organization of the fibroblast lineage. *Nature*. 593:575–579. <https://doi.org/10.1038/s41586-021-03549-5>
- Butzow, J.J., and G.L. Eichhorn. 1968. Physical chemical studies on the age changes in rat tail tendon collagen. *Biochim. Biophys. Acta.* 154:208–219. [https://doi.org/10.1016/0005-2795\(68\)90273-0](https://doi.org/10.1016/0005-2795(68)90273-0)
- Carver, W., L. Terracio, and T.K. Borg. 1993. Expression and accumulation of interstitial collagen in the neonatal rat heart. *Anat. Rec.* 236:511–520. <https://doi.org/10.1002/ar.1092360311>
- Chan, K.M., H.L. Wong, G. Jin, B. Liu, R. Cao, Y. Cao, K. Lehti, K. Tryggvason, and Z. Zhou. 2012. MT1-MMP inactivates ADAM9 to regulate FGFR2 signaling and calvarial osteogenesis. *Dev. Cell.* 22:1176–1190. <https://doi.org/10.1016/j.devcel.2012.04.014>
- Chang, H.Y., J.T. Chi, S. Dudoit, C. Bondre, M. van de Rijn, D. Botstein, and P.O. Brown. 2002. Diversity, topographic differentiation, and positional memory in human fibroblasts. *Proc. Natl. Acad. Sci. USA.* 99:12877–12882. <https://doi.org/10.1073/pnas.162488599>
- Chun, T.H., F. Sabeh, I. Ota, H. Murphy, K.T. McDonagh, K. Holmbeck, H. Birkedal-Hansen, E.D. Allen, and S.J. Weiss. 2004. MT1-MMP-dependent

- neovessel formation within the confines of the three-dimensional extracellular matrix. *J. Cell Biol.* 167:757–767. <https://doi.org/10.1083/jcb.200405001>
- Chun, T.H., K.B. Hotary, F. Sabeh, A.R. Saltiel, E.D. Allen, and S.J. Weiss. 2006. A pericellular collagenase directs the 3-dimensional development of white adipose tissue. *Cell.* 125:577–591. <https://doi.org/10.1016/j.cell.2006.02.050>
- Creemers, L.B., D.C. Jansen, A. van Veen-Reurings, T. van den Bos, and V. Everts. 1997. Microassay for the assessment of low levels of hydroxyproline. *Biotechniques.* 22:656–658. <https://doi.org/10.2144/97224bm19>
- Crewe, C., N. Joffin, J.M. Rutkowski, M. Kim, F. Zhang, D.A. Towler, R. Gordillo, and P.E. Scherer. 2018. An endothelial-to-adipocyte extracellular vesicle axis governed by metabolic state. *Cell.* 175:695–708.e13. <https://doi.org/10.1016/j.cell.2018.09.005>
- Darby, I.A., T. Bisucci, B. Pittet, S. Garbin, G. Gabbiani, and A. Desmoulière. 2002. Skin flap-induced regression of granulation tissue correlates with reduced growth factor and increased metalloproteinase expression. *J. Pathol.* 197:117–127. <https://doi.org/10.1002/path.1074>
- Dobin, A., C.A. Davis, F. Schlesinger, J. Drenkow, C. Zaleski, S. Jha, P. Batut, M. Chaisson, and T.R. Gingeras. 2013. STAR: Ultrafast universal RNA-seq aligner. *Bioinformatics.* 29:15–21. <https://doi.org/10.1093/bioinformatics/bts635>
- Driskell, R.R., and F.M. Watt. 2015. Understanding fibroblast heterogeneity in the skin. *Trends Cell Biol.* 25:92–99. <https://doi.org/10.1016/j.tcb.2014.10.001>
- Driskell, R.R., B.M. Lichtenberger, E. Hoste, K. Kretzschmar, B.D. Simons, M. Charalambous, S.R. Ferron, Y. Haurault, G. Pavlovic, A.C. Ferguson-Smith, et al. 2013. Distinct fibroblast lineages determine dermal architecture in skin development and repair. *Nature.* 504:277–281. <https://doi.org/10.1038/nature12783>
- Dudley, D.T., X.-Y. Li, C.Y. Hu, C.G. Kleer, A.L. Willis, and S.J. Weiss. 2014. A 3D matrix platform for the rapid generation of therapeutic anti-human carcinoma monoclonal antibodies. *Proc. Natl. Acad. Sci. U S A.* 111:14882–14887. <https://doi.org/10.1073/pnas.1410996111>
- Ewald, C.Y., J.N. Landis, J. Porter Abate, C.T. Murphy, and T.K. Blackwell. 2015. Dauer-independent insulin/IGF-1-signalling implicates collagen remodeling in longevity. *Nature.* 519:97–101. <https://doi.org/10.1038/nature14021>
- Ewels, P., M. Magnusson, S. Lundin, and M. Källér. 2016. MultiQC: Summarize analysis results for multiple tools and samples in a single report. *Bioinformatics.* 32:3047–3048. <https://doi.org/10.1093/bioinformatics/btw354>
- Feinberg, T.Y., R.G. Rowe, T.L. Saunders, and S.J. Weiss. 2016. Functional roles of MMP14 and MMP15 in early postnatal mammary gland development. *Development.* 143:3956–3968. <https://doi.org/10.1242/dev.136259>
- Feinberg, T.Y., H. Zheng, R. Liu, M.S. Wicha, S.M. Yu, and S.J. Weiss. 2018. Divergent matrix-remodeling strategies distinguish developmental from neoplastic mammary epithelial cell invasion programs. *Dev. Cell.* 47:145–160.e6. <https://doi.org/10.1016/j.devcel.2018.08.025>
- Fields, G.B. 2013. Interstitial collagen catabolism. *J. Biol. Chem.* 288:8785–8793. <https://doi.org/10.1074/jbc.R113.451211>
- Filippov, S., G.C. Koenig, T.H. Chun, K.B. Hotary, I. Ota, T.H. Bugge, J.D. Roberts, W.P. Fay, H. Birkedal-Hansen, K. Holmbeck, et al. 2005. MT1-matrix metalloproteinase directs arterial wall invasion and neointima formation by vascular smooth muscle cells. *J. Exp. Med.* 202:663–671. <https://doi.org/10.1084/jem.20050607>
- Folkman, J., and A. Moscona. 1978. Role of cell shape in growth control. *Nature.* 273:345–349. <https://doi.org/10.1038/273345a0>
- Gelman, R.A., D.C. Poppke, and K.A. Piez. 1979. Collagen fibril formation in vitro. The role of the nonhelical terminal regions. *J. Biol. Chem.* 254:11741–11745. [https://doi.org/10.1016/S0021-9258\(19\)86545-6](https://doi.org/10.1016/S0021-9258(19)86545-6)
- Gonzalo, P., M.C. Guadamillas, M.V. Hernández-Riquer, A. Pollán, A. Grande-García, R.A. Bartolomé, A. Vasanji, C. Ambrogio, R. Chiarle, J. Teixidó, et al. 2010. MT1-MMP is required for myeloid cell fusion via regulation of Rac1 signaling. *Dev. Cell.* 18:77–89. <https://doi.org/10.1016/j.devcel.2009.11.012>
- Grinnell, F., and W.M. Petroll. 2010. Cell motility and mechanics in three-dimensional collagen matrices. *Annu. Rev. Cell Dev. Biol.* 26:335–361. <https://doi.org/10.1146/annurev.cellbio.042308.113318>
- Grinnell, F., C.H. Ho, E. Tamariz, D.J. Lee, and G. Skuta. 2003. Dendritic fibroblasts in three-dimensional collagen matrices. *Mol. Biol. Cell.* 14:384–395. <https://doi.org/10.1091/mbc.e02-08-0493>
- Gutiérrez-Fernández, A., C. Soria-Valles, F.G. Osorio, J. Gutiérrez-Abril, C. Garabayo, A. Aguirre, A. Fueyo, M.S. Fernández-García, X.S. Puente, and C. López-Otin. 2015. Loss of MT1-MMP causes cell senescence and nuclear defects which can be reversed by retinoic acid. *EMBO J.* 34:1875–1888. <https://doi.org/10.15252/emj.201490594>

- Han, Y.L., P. Ronceray, G. Xu, A. Malandrino, R.D. Kamm, M. Lenz, C.P. Broedersz, and M. Guo. 2018. Cell contraction induces long-ranged stress stiffening in the extracellular matrix. *Proc. Natl. Acad. Sci. USA*. 115:4075–4080. <https://doi.org/10.1073/pnas.1722619115>
- Holmbeck, K., P. Bianco, J. Caterina, S. Yamada, M. Kromer, S.A. Kuznetsov, M. Mankani, P.G. Robey, A.R. Poole, I. Pidoux, et al. 1999. MT1-MMP-deficient mice develop dwarfism, osteopenia, arthritis, and connective tissue disease due to inadequate collagen turnover. *Cell*. 99:81–92. [https://doi.org/10.1016/S0092-8674\(00\)80064-1](https://doi.org/10.1016/S0092-8674(00)80064-1)
- Holmbeck, K., P. Bianco, I. Pidoux, S. Inoue, R.C. Billingham, W. Wu, K. Chrysovergis, S. Yamada, H. Birkedal-Hansen, and A.R. Poole. 2005. The metalloproteinase MT1-MMP is required for normal development and maintenance of osteocyte processes in bone. *J. Cell Sci*. 118:147–156. <https://doi.org/10.1242/jcs.01581>
- Hotary, K.B., I. Yana, F. Sabeh, X.Y. Li, K. Holmbeck, H. Birkedal-Hansen, E.D. Allen, N. Hiraoka, and S.J. Weiss. 2002. Matrix metalloproteinases (MMPs) regulate fibrin-invasive activity via MT1-MMP-dependent and -independent processes. *J. Exp. Med*. 195:295–308. <https://doi.org/10.1084/jem.20010815>
- Hotary, K.B., E.D. Allen, P.C. Brooks, N.S. Datta, M.W. Long, and S.J. Weiss. 2003. Membrane type I matrix metalloproteinase usurps tumor growth control imposed by the three-dimensional extracellular matrix. *Cell*. 114:33–45. [https://doi.org/10.1016/S0092-8674\(03\)00513-0](https://doi.org/10.1016/S0092-8674(03)00513-0)
- Itoh, Y. 2015. Membrane-type matrix metalloproteinases: Their functions and regulations. *Matrix Biol*. 44–46:207–223. <https://doi.org/10.1016/j.matbio.2015.03.004>
- Jin, G., F. Zhang, K.M. Chan, H.L. Xavier Wong, B. Liu, K.S. Cheah, X. Liu, C. Mauch, D. Liu, and Z. Zhou. 2011. MT1-MMP cleaves Dll1 to negatively regulate Notch signalling to maintain normal B-cell development. *EMBO J*. 30:2281–2293. <https://doi.org/10.1038/emboj.2011.136>
- Kalson, N.S., Y. Lu, S.H. Taylor, T. Starborg, D.F. Holmes, and K.E. Kadler. 2015. A structure-based extracellular matrix expansion mechanism of fibrous tissue growth. *Elife*. 4:e05958. <https://doi.org/10.7554/eLife.05958>
- Karsdal, M.A., T.A. Andersen, L. Bonewald, and C. Christiansen. 2004. Matrix metalloproteinases (MMPs) safeguard osteoblasts from apoptosis during transdifferentiation into osteocytes: MT1-MMP maintains osteocyte viability. *DNA Cell Biol*. 23:155–165. <https://doi.org/10.1089/104454904322964751>
- Keene, D.R., L.Y. Sakai, H.P. Bächinger, and R.E. Burgeson. 1987. Type III collagen can be present on banded collagen fibrils regardless of fibril diameter. *J. Cell Biol*. 105:2393–2402. <https://doi.org/10.1083/jcb.105.5.2393>
- Klein, L., and J. ChandraRajan. 1977. Collagen degradation in rat skin but not in intestine during rapid growth: Effect on collagen types I and III from skin. *Proc. Natl. Acad. Sci. USA*. 74:1436–1439. <https://doi.org/10.1073/pnas.74.4.1436>
- Kobayashi, T., X. Liu, H.J. Kim, T. Kohyama, F.Q. Wen, S. Abe, Q. Fang, Y.K. Zhu, J.R. Spurzem, P. Bitterman, and S.I. Rennard. 2005. TGF-beta1 and serum both stimulate contraction but differentially affect apoptosis in 3D collagen gels. *Respir. Res*. 6:141. <https://doi.org/10.1186/1465-9921-6-141>
- Koenig, G.C., R.G. Rowe, S.M. Day, F. Sabeh, J.J. Atkinson, K.R. Cooke, and S.J. Weiss. 2012. MT1-MMP-dependent remodeling of cardiac extracellular matrix structure and function following myocardial infarction. *Am. J. Pathol*. 180:1863–1878. <https://doi.org/10.1016/j.ajpath.2012.01.022>
- Kotlarchyk, M.A., S.G. Shreim, M.B. Alvarez-Elizondo, L.C. Estrada, R. Singh, L. Valdevit, E. Kniazeva, E. Gratton, A.J. Putnam, and E.L. Botvinick. 2011. Concentration independent modulation of local micromechanics in a fibrin gel. *PLoS One*. 6:e20201. <https://doi.org/10.1371/journal.pone.0020201>
- Koyama, H., E.W. Raines, K.E. Bornfeldt, J.M. Roberts, and R. Ross. 1996. Fibrillar collagen inhibits arterial smooth muscle proliferation through regulation of Cdk2 inhibitors. *Cell*. 87:1069–1078. [https://doi.org/10.1016/S0092-8674\(00\)81801-2](https://doi.org/10.1016/S0092-8674(00)81801-2)
- Lakshman, N., and W.M. Petroll. 2012. Growth factor regulation of corneal keratocyte mechanical phenotypes in 3-D collagen matrices. *Invest. Ophthalmol. Vis. Sci*. 53:1077–1086. <https://doi.org/10.1167/iovs.11-8609>
- Lee, Y.H., and W.P. Schiemann. 2011. Fibromodulin suppresses nuclear factor-kappaB activity by inducing the delayed degradation of IKBA via a JNK-dependent pathway coupled to fibroblast apoptosis. *J. Biol. Chem*. 286:6414–6422. <https://doi.org/10.1074/jbc.M110.168682>
- Lee, J., A.A. Abdeen, and K.A. Kilian. 2014. Rewiring mesenchymal stem cell lineage specification by switching the biophysical microenvironment. *Sci. Rep*. 4:5188. <https://doi.org/10.1038/srep05188>
- Lehti, K., E. Allen, H. Birkedal-Hansen, K. Holmbeck, Y. Miyake, T.H. Chun, and S.J. Weiss. 2005. An MT1-MMP-PDGF receptor-beta axis regulates mural cell investment of the microvasculature. *Genes Dev*. 19:979–991. <https://doi.org/10.1101/gad.1294605>
- Lei, K., A. Nimnual, W.X. Zong, N.J. Kennedy, R.A. Flavell, C.B. Thompson, D. Bar-Sagi, and R.J. Davis. 2002. The Bax subfamily of Bcl2-related proteins is essential for apoptotic signal transduction by c-Jun NH(2)-terminal kinase. *Mol. Cell. Biol*. 22:4929–4942. <https://doi.org/10.1128/MCB.22.13.4929-4942.2002>
- Leight, J.L., M.A. Wozniak, S. Chen, M.L. Lynch, and C.S. Chen. 2012. Matrix rigidity regulates a switch between TGF-beta1-induced apoptosis and epithelial-mesenchymal transition. *Mol. Biol. Cell*. 23:781–791. <https://doi.org/10.1091/mbc.e11-06-0537>
- Li, B., and C.N. Dewey. 2011. RSEM: Accurate transcript quantification from RNA-seq data with or without a reference genome. *BMC Bioinformatics*. 12:323. <https://doi.org/10.1186/1471-2105-12-323>
- Li, X.Y., I. Ota, I. Yana, F. Sabeh, and S.J. Weiss. 2008. Molecular dissection of the structural machinery underlying the tissue-invasive activity of membrane type-1 matrix metalloproteinase. *Mol. Biol. Cell*. 19:3221–3233. <https://doi.org/10.1091/mbc.e08-01-0016>
- Liu, X., H. Wu, M. Byrne, J. Jeffrey, S. Krane, and R. Jaenisch. 1995. A targeted mutation at the known collagenase cleavage site in mouse type I collagen impairs tissue remodeling. *J. Cell Biol*. 130:227–237. <https://doi.org/10.1083/jcb.130.1.227>
- Löhler, J., R. Timpl, and R. Jaenisch. 1984. Embryonic lethal mutation in mouse collagen I gene causes rupture of blood vessels and is associated with erythropoietic and mesenchymal cell death. *Cell*. 38:597–607. [https://doi.org/10.1016/0092-8674\(84\)90514-2](https://doi.org/10.1016/0092-8674(84)90514-2)
- Love, M.I., W. Huber, and S. Anders. 2014. Moderated estimation of fold change and dispersion for RNA-seq data with DESeq2. *Genome Biol*. 15:550. <https://doi.org/10.1186/s13059-014-0550-8>
- Madsen, D.H., L.H. Engelholm, S. Ingvarsen, T. Hillig, R.A. Wagenaar-Miller, L. Kjoller, H. Gårdsvoll, G. Høyer-Hansen, K. Holmbeck, T.H. Bugge, and N. Brendt. 2007. Extracellular collagenases and the endocytic receptor, urokinase plasminogen activator receptor-associated protein/Endo180, cooperate in fibroblast-mediated collagen degradation. *J. Biol. Chem*. 282:27037–27045. <https://doi.org/10.1074/jbc.M701088200>
- Maeda, T., T. Sakabe, A. Sunaga, K. Sakai, A.L. Rivera, D.R. Keene, T. Sasaki, E. Stavnezer, J. Iannotti, R. Schweitzer, et al. 2011. Conversion of mechanical force into TGF-beta-mediated biochemical signals. *Curr. Biol*. 21:933–941. <https://doi.org/10.1016/j.cub.2011.04.007>
- Mao, J.R., G. Taylor, W.B. Dean, D.R. Wagner, V. Afzal, J.C. Lotz, E.M. Rubin, and J. Bristow. 2002. Tenascin-X deficiency mimics Ehlers-Danlos syndrome in mice through alteration of collagen deposition. *Nat. Genet*. 30:421–425. <https://doi.org/10.1038/ng850>
- Maquoi, E., D. Assent, J. Detilleux, C. Pequeux, J.M. Foidart, and A. Noël. 2012. MT1-MMP protects breast carcinoma cells against type I collagen-induced apoptosis. *Oncogene*. 31:480–493. <https://doi.org/10.1038/onc.2011.249>
- Martin, M. 2011. Cutadapt removes adapter sequences from high-throughput sequencing reads. *EMBnet. J*. 17:10. <https://doi.org/10.14806/ej.17.1.200>
- Massagué, J. 2012. TGFbeta signalling in context. *Nat. Rev. Mol. Cell Biol*. 13:616–630. <https://doi.org/10.1038/nrm3434>
- Mays, P.K., J.E. Bishop, and G.J. Laurent. 1988. Age-related changes in the proportion of types I and III collagen. *Mech. Ageing Dev*. 45:203–212. [https://doi.org/10.1016/0047-6374\(88\)90002-4](https://doi.org/10.1016/0047-6374(88)90002-4)
- Montgomery, A.M., R.A. Reisfeld, and D.A. Cheresch. 1994. Integrin alpha v beta 3 rescues melanoma cells from apoptosis in three-dimensional dermal collagen. *Proc. Natl. Acad. Sci. USA*. 91:8856–8860. <https://doi.org/10.1073/pnas.91.19.8856>
- Morishige, N., W.M. Petroll, T. Nishida, M.C. Kenney, and J.V. Jester. 2006. Noninvasive corneal stromal collagen imaging using two-photon-generated second-harmonic signals. *J. Cataract Refract. Surg*. 32:1784–1791. <https://doi.org/10.1016/j.jcrs.2006.08.027>
- Nho, R.S., H. Xia, J. Kahm, J. Kleidon, D. Diebold, and C.A. Henke. 2005. Role of integrin-linked kinase in regulating phosphorylation of Akt and fibroblast survival in type I collagen matrices through a beta1 integrin viability signaling pathway. *J. Biol. Chem*. 280:26630–26639. <https://doi.org/10.1074/jbc.M411798200>
- Nicholson, D.W. 2000. From bench to clinic with apoptosis-based therapeutic agents. *Nature*. 407:810–816. <https://doi.org/10.1038/35037747>
- Niland, S., A. Cremer, J. Fluck, J.A. Eble, T. Krieg, and S. Sollberg. 2001. Contraction-dependent apoptosis of normal dermal fibroblasts. *J. Invest. Dermatol*. 116:686–692. <https://doi.org/10.1046/j.1523-1747.2001.01342.x>
- Ohuchi, E., K. Imai, Y. Fujii, H. Sato, M. Seiki, and Y. Okada. 1997. Membrane type 1 matrix metalloproteinase digests interstitial collagens and other

- extracellular matrix macromolecules. *J. Biol. Chem.* 272:2446–2451. <https://doi.org/10.1074/jbc.272.4.2446>
- Orgel, J.P., T.C. Irving, A. Miller, and T.J. Wess. 2006. Microfibrillar structure of type I collagen in situ. *Proc. Natl. Acad. Sci. USA.* 103:9001–9005. <https://doi.org/10.1073/pnas.0502718103>
- Perumal, S., O. Antipova, and J.P. Orgel. 2008. Collagen fibril architecture, domain organization, and triple-helical conformation govern its proteolysis. *Proc. Natl. Acad. Sci. USA.* 105:2824–2829. <https://doi.org/10.1073/pnas.0710588105>
- Rinn, J.L., C. Bondre, H.B. Gladstone, P.O. Brown, and H.Y. Chang. 2006. Anatomical demarcation by positional variation in fibroblast gene expression programs. *PLoS Genet.* 2:e119. <https://doi.org/10.1371/journal.pgen.0020119>
- Rognoni, E., and F.M. Watt. 2018. Skin cell heterogeneity in development, wound healing, and cancer. *Trends Cell Biol.* 28:709–722. <https://doi.org/10.1016/j.tcb.2018.05.002>
- Rowe, R.G., and S.J. Weiss. 2009. Navigating ECM barriers at the invasive front: The cancer cell-stroma interface. *Annu. Rev. Cell Dev. Biol.* 25: 567–595. <https://doi.org/10.1146/annurev.cellbio.24.110707.175315>
- Rowe, R.G., D. Keena, F. Sabeh, A.L. Willis, and S.J. Weiss. 2011. Pulmonary fibroblasts mobilize the membrane-tethered matrix metalloproteinase, MT1-MMP, to destructively remodel and invade interstitial type I collagen barriers. *Am. J. Physiol. Lung Cell. Mol. Physiol.* 301:L683–L692. <https://doi.org/10.1152/ajplung.00187.2011>
- Rys, J.P., C.C. DuFort, D.A. Monteiro, M.A. Baird, J.A. Oses-Prieto, S. Chand, A.L. Burlingame, M.W. Davidson, and T.N. Alliston. 2015. Discrete spatial organization of TGF β receptors couples receptor multimerization and signaling to cellular tension. *Elife.* 4:e09300. <https://doi.org/10.7554/eLife.09300>
- Sabeh, F., I. Ota, K. Holmbeck, H. Birkedal-Hansen, P. Soloway, M. Balbin, C. Lopez-Otin, S. Shapiro, M. Inada, S. Krane, et al. 2004. Tumor cell traffic through the extracellular matrix is controlled by the membrane-anchored collagenase MT1-MMP. *J. Cell Biol.* 167:769–781. <https://doi.org/10.1083/jcb.200408028>
- Sabeh, F., X.Y. Li, T.L. Saunders, R.G. Rowe, and S.J. Weiss. 2009a. Secreted versus membrane-anchored collagenases: Relative roles in fibroblast-dependent collagenolysis and invasion. *J. Biol. Chem.* 284:23001–23011. <https://doi.org/10.1074/jbc.M109.002808>
- Sabeh, F., R. Shimizu-Hirota, and S.J. Weiss. 2009b. Protease-dependent versus -independent cancer cell invasion programs: Three-dimensional amoeboid movement revisited. *J. Cell Biol.* 185:11–19. <https://doi.org/10.1083/jcb.200807195>
- Sakamoto, T., J.S. Weng, T. Hara, S. Yoshino, H. Kozuka-Hata, M. Oyama, and M. Seiki. 2014. Hypoxia-inducible factor 1 regulation through cross talk between mTOR and MT1-MMP. *Mol. Cell. Biol.* 34:30–42. <https://doi.org/10.1128/MCB.01169-13>
- Sakr, M., X.Y. Li, F. Sabeh, T.Y. Feinberg, J.J.G. Tesmer, Y. Tang, and S.J. Weiss. 2018. Tracking the Cartoon mouse phenotype: Hemopexin domain-dependent regulation of MT1-MMP pericellular collagenolytic activity. *J. Biol. Chem.* 293:8113–8127. <https://doi.org/10.1074/jbc.RA117.001503>
- Schuster, N., N. Dünker, and K. Kriegelstein. 2002. Transforming growth factor- β induced cell death in the developing chick retina is mediated via activation of c-jun N-terminal kinase and downregulation of the anti-apoptotic protein Bcl-X(L). *Neurosci. Lett.* 330:239–242. [https://doi.org/10.1016/S0304-3940\(02\)00801-7](https://doi.org/10.1016/S0304-3940(02)00801-7)
- Sherman, B.T., M. Hao, J. Qiu, X. Jiao, M.W. Baseler, H.C. Lane, T. Imamichi, and W. Chang. 2022. DAVID: A web server for functional enrichment analysis and functional annotation of gene lists (2021 update). *Nucleic Acids Res.* 50:W216–W221. <https://doi.org/10.1093/nar/gkac194>
- Shihan, M.H., S.G. Novo, S.J. Le Marchand, Y. Wang, and M.K. Duncan. 2021. A simple method for quantitating confocal fluorescent images. *Biochem. Biophys. Rep.* 25:100916. <https://doi.org/10.1016/j.bbrep.2021.100916>
- Shimizu-Hirota, R., W. Xiong, B.T. Baxter, S.L. Kunkel, I. Maillard, X.W. Chen, F. Sabeh, R. Liu, X.Y. Li, and S.J. Weiss. 2012. MT1-MMP regulates the PI3K δ -Mi-2/NuRD-dependent control of macrophage immune function. *Genes Dev.* 26:395–413. <https://doi.org/10.1101/gad.178749.111>
- Shimoda, M., and R. Khokha. 2017. Metalloproteinases in extracellular vesicles. *Biochim. Biophys. Acta Mol. Cell Res.* 1864:1989–2000. <https://doi.org/10.1016/j.bbamcr.2017.05.027>
- Smith, L.T., K.A. Holbrook, and P.H. Byers. 1982. Structure of the dermal matrix during development and in the adult. *J. Invest. Dermatol.* 79: 93s–104s. <https://doi.org/10.1111/1523-1747.ep12545877>
- Tang, Y., R.G. Rowe, E.L. Botvinick, A. Kurup, A.J. Putnam, M. Seiki, V.M. Weaver, E.T. Keller, S. Goldstein, J. Dai, et al. 2013. MT1-MMP-dependent control of skeletal stem cell commitment via a β 1-integrin/YAP/TAZ signaling axis. *Dev. Cell.* 25:402–416. <https://doi.org/10.1016/j.devcel.2013.04.011>
- Tang, Y., L. Zhu, J.S. Cho, X.Y. Li, and S.J. Weiss. 2022. Matrix remodeling controls a nuclear lamin A/C-emerin network that directs Wnt-regulated stem cell fate. *Dev. Cell.* 57:480–495.e6. <https://doi.org/10.1016/j.devcel.2022.01.015>
- Taylor, S.H., C.Y. Yeung, N.S. Kalson, Y. Lu, P. Zigrino, T. Starborg, S. Warwood, D.F. Holmes, E.G. Canty-Laird, C. Mauch, and K.E. Kadler. 2015. Matrix metalloproteinase 14 is required for fibrous tissue expansion. *Elife.* 4:e09345. <https://doi.org/10.7554/eLife.09345>
- Valacca, C., E. Tassone, and P. Mignatti. 2015. TIMP-2 interaction with MT1-MMP activates the AKT pathway and protects tumor cells from apoptosis. *PLoS One.* 10:e0136797. <https://doi.org/10.1371/journal.pone.0136797>
- Varedi, M., E.E. Tredget, A. Ghahary, and P.G. Scott. 2000. Stress-relaxation and contraction of a collagen matrix induces expression of TGF- β and triggers apoptosis in dermal fibroblasts. *Biochem. Cell Biol.* 78: 427–436. <https://doi.org/10.1139/o00-014>
- Wall, S.J., Z.D. Zhong, and Y.A. DeClerck. 2007. The cyclin-dependent kinase inhibitors p15INK4B and p21CIP1 are critical regulators of fibrillar collagen-induced tumor cell cycle arrest. *J. Biol. Chem.* 282:24471–24476. <https://doi.org/10.1074/jbc.M702697200>
- Wang, H.B., M. Dembo, and Y.L. Wang. 2000. Substrate flexibility regulates growth and apoptosis of normal but not transformed cells. *Am. J. Physiol. Cell Physiol.* 279:C1345–C1350. <https://doi.org/10.1152/ajpcell.2000.279.5.C1345>
- Wang, Y.H., W.T. Chiu, Y.K. Wang, C.C. Wu, T.L. Chen, C.F. Teng, W.T. Chang, H.C. Chang, and M.J. Tang. 2007. Deregulation of AP-1 proteins in collagen gel-induced epithelial cell apoptosis mediated by low substratum rigidity. *J. Biol. Chem.* 282:752–763. <https://doi.org/10.1074/jbc.M604801200>
- Wolf, K., M. Te Lindert, M. Krause, S. Alexander, J. Te Riet, A.L. Willis, R.M. Hoffman, C.G. Figdor, S.J. Weiss, and P. Friedl. 2013. Physical limits of cell migration: Control by ECM space and nuclear deformation and tuning by proteolysis and traction force. *J. Cell Biol.* 201:1069–1084. <https://doi.org/10.1083/jcb.201210152>
- Xia, X.D., G. Gill, H. Lin, D.M. Roth, H.M. Gu, X.J. Wang, F.Y. Su, A. Alabi, M. Alexiou, Z. Zhang, et al. 2023. Global, but not chondrocyte-specific, MT1-MMP deficiency in adult mice causes inflammatory arthritis. *Matrix Biol.* 122:10–17. <https://doi.org/10.1016/j.matbio.2023.08.003>
- Yana, I., H. Sagara, S. Takaki, K. Takatsu, K. Nakamura, K. Nakao, M. Katsuki, S. Taniguchi, T. Aoki, H. Sato, et al. 2007. Crosstalk between neovessels and mural cells directs the site-specific expression of MT1-MMP to endothelial tip cells. *J. Cell Sci.* 120:1607–1614. <https://doi.org/10.1242/jcs.000679>
- Yang, C., M.W. Tibbitt, L. Basta, and K.S. Anseth. 2014. Mechanical memory and dosing influence stem cell fate. *Nat. Mater.* 13:645–652. <https://doi.org/10.1038/nmat3889>
- Zhou, C., and W.M. Petroll. 2014. MMP regulation of corneal keratocyte motility and mechanics in 3-D collagen matrices. *Exp. Eye Res.* 121: 147–160. <https://doi.org/10.1016/j.exer.2014.02.002>
- Zhou, Z., S.S. Apte, R. Soininen, R. Cao, G.Y. Baaklini, R.W. Rausser, J. Wang, Y. Cao, and K. Tryggvason. 2000. Impaired endochondral ossification and angiogenesis in mice deficient in membrane-type matrix metalloproteinase I. *Proc. Natl. Acad. Sci. USA.* 97:4052–4057. <https://doi.org/10.1073/pnas.060037197>
- Zhou, X., A. Jamil, A. Nash, J. Chan, N. Trim, J.P. Iredale, and R.C. Benyon. 2006. Impaired proteolysis of collagen I inhibits proliferation of hepatic stellate cells: Implications for regulation of liver fibrosis. *J. Biol. Chem.* 281:39757–39765. <https://doi.org/10.1074/jbc.M605621200>
- Zigrino, P., J. Brinckmann, A. Niehoff, Y. Lu, N. Giebeler, B. Eckes, K.E. Kadler, and C. Mauch. 2016. Fibroblast-derived MMP-14 regulates collagen homeostasis in adult skin. *J. Invest. Dermatol.* 136:1575–1583. <https://doi.org/10.1016/j.jid.2016.03.036>
- Zucker, S., M. Drews, C. Conner, H.D. Foda, Y.A. DeClerck, K.E. Langley, W.F. Bahou, A.J. Docherty, and J. Cao. 1998. Tissue inhibitor of metalloproteinase-2 (TIMP-2) binds to the catalytic domain of the cell surface receptor, membrane type 1-matrix metalloproteinase 1 (MT1-MMP). *J. Biol. Chem.* 273:1216–1222. <https://doi.org/10.1074/jbc.273.2.1216>

Supplemental material

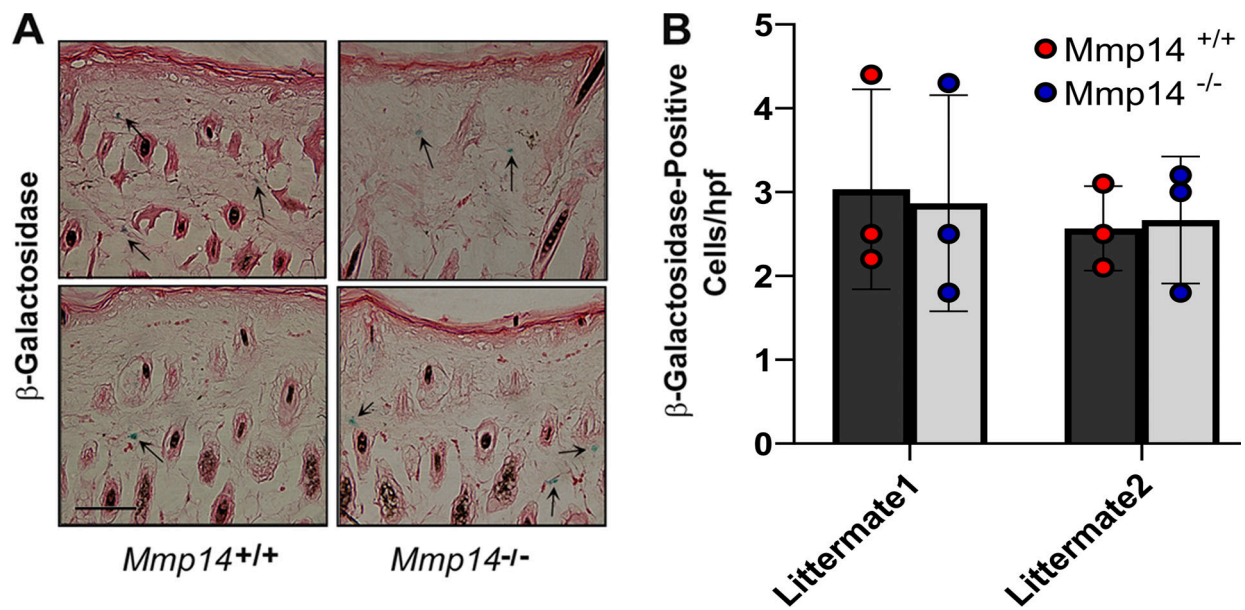


Figure S1. ***Mmp14*-dependent control of dermal fibroblast senescence.** (A) Representative micrographs of β -galactosidase staining (pH 6.0) of dorsal skin isolated from 18-day-old *Mmp14^{+/+}* or *Mmp14^{-/-}* littermates (black arrows demarcate senescent cells) (bar = 200 μ m). (B) Senescent cells were quantified in 10 or more randomly selected high power fields in three pairs of *Mmp14^{+/+}* or *Mmp14^{-/-}* littermates (mean \pm SEM).

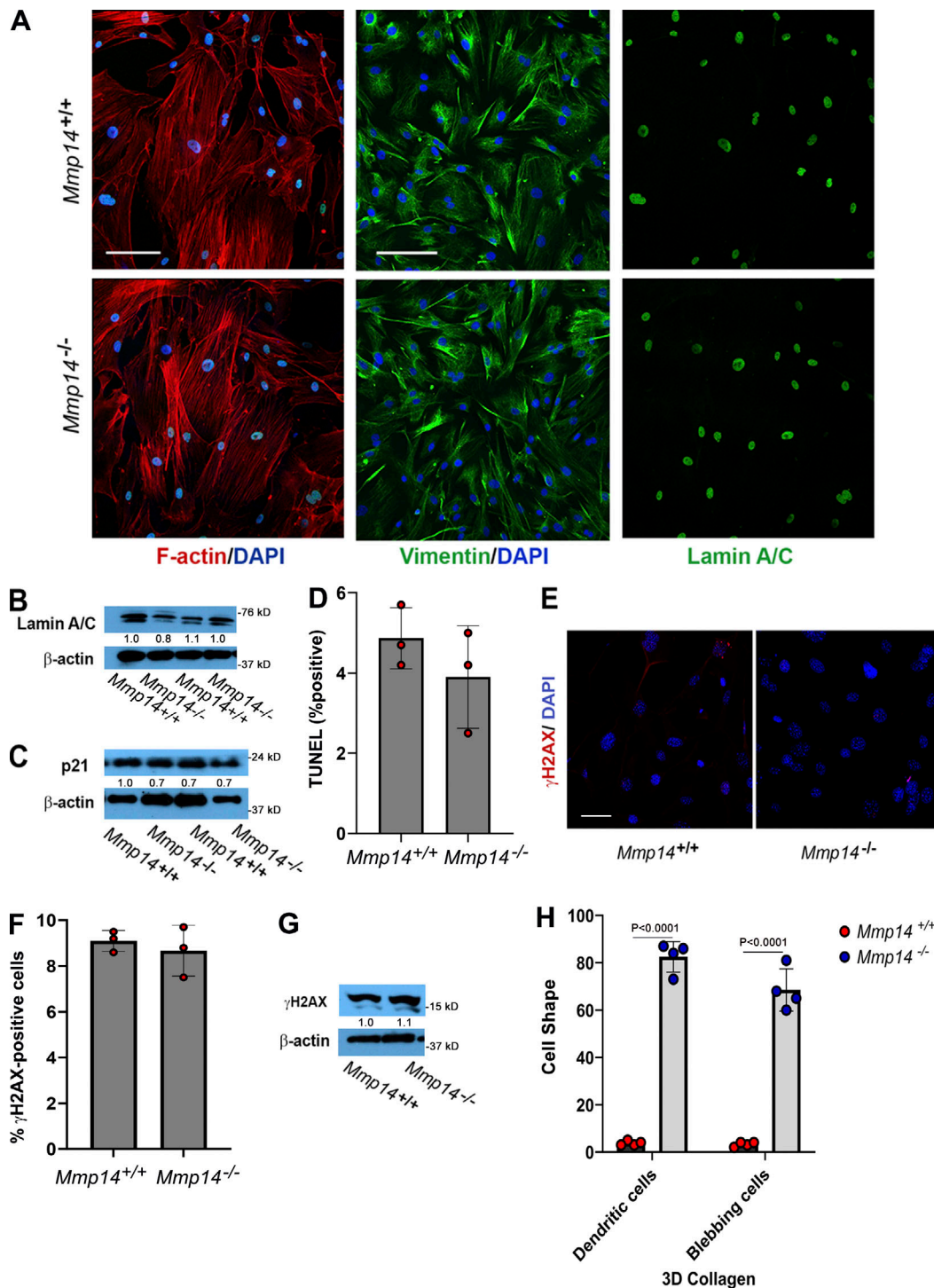


Figure S2. **Mmp14-dependent regulation of fibroblast function in 2-D culture.** (A) Confocal images of *Mmp14^{+/+}* and *Mmp14^{-/-}* fibroblasts were cultured atop cover glass slips and stained for F-actin with phalloidin (DAPI counterstain), vimentin, or lamin A/C (bar = 50 μ m). (B) Western blot analysis of lamin A/C expression in *Mmp14^{+/+}* fibroblasts relative to *Mmp14^{-/-}* fibroblasts with GAPDH used as the loading control. Relative expression levels are shown as determined by densitometry. (C) p21 expression levels as assessed by western blot analysis in *Mmp14^{+/+}* versus *Mmp14^{-/-}* fibroblasts with GAPDH used as the loading control. Relative expression levels are shown as determined by densitometry. (D) *Mmp14^{+/+}* and *Mmp14^{-/-}* fibroblasts were cultured atop type I collagen hydrogels (identical to those used for 3-D culture) for 5 days and monitored for TUNEL staining (mean \pm SEM; $n = 3$ independent experiments) as determined by Student's t test. (E and F) Immunofluorescence staining of γ -H2AX in fibroblasts isolated from *Mmp14^{+/+}* and *Mmp14^{-/-}* littermates (bar = 50 μ m) (E) with the percentage of γ -H2AX-positive nuclei (mean \pm SEM with P value determined by Student's t test) quantified in 10 randomly selected high-powered fields from three independent experiments (F). (G) γ -H2AX protein expression levels in *Mmp14^{+/+}* or *Mmp14^{-/-}* fibroblasts in 2-D culture as quantified by western blot, using β -actin as the loading control. Relative expression levels are shown as determined by densitometry. (H) *Mmp14* wild-type and knockout cells were cultured in 3-D collagen hydrogels and the percent dendritic and blebbing cells quantified in 10 random fields in four independent experiments with results presented as mean \pm SEM with P value determined by Student's t test. Source data are available for this figure: SourceData FS2.

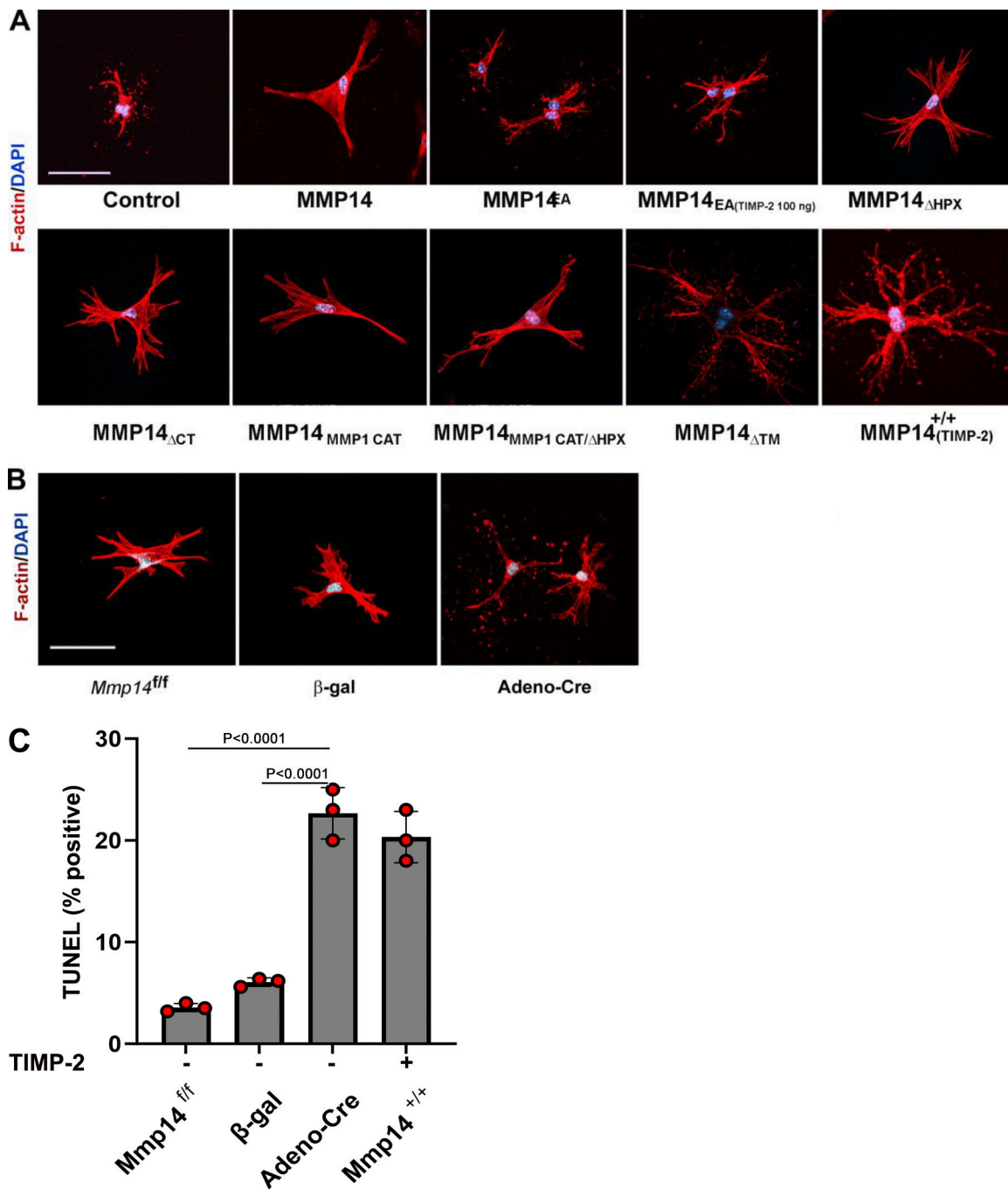


Figure S3. **Mmp14-dependent pericellular proteolysis and the regulation of fibroblast survival.** (A) *Mmp14*^{-/-} fibroblasts were transduced with a control expression vector, wild-type, or mutant MMP14 constructs as described in Fig. 3 and cultured for 5 days in 3-D collagen hydrogels prior to in situ F-actin/nuclear staining (bar = 100 μm). Results are representative of three experiments performed. (B and C) Dermal fibroblasts isolated from *Mmp14*^{fl/fl} mice were transduced with adeno-βgal or adeno-Cre expression vectors and embedded in collagen hydrogels for 5 day before F-actin (B) (bar = 100 μm) or TUNEL staining/quantification (mean ± SEM; n = 3 independent experiments) (C). The ability of TIMP-2 (3 μg/ml) to induce apoptosis in *Mmp14*^{+/+} fibroblasts is shown in panel C. Mean ± SEM (n = 3 independent experiments). One-way ANOVA and Dunett's post-test.

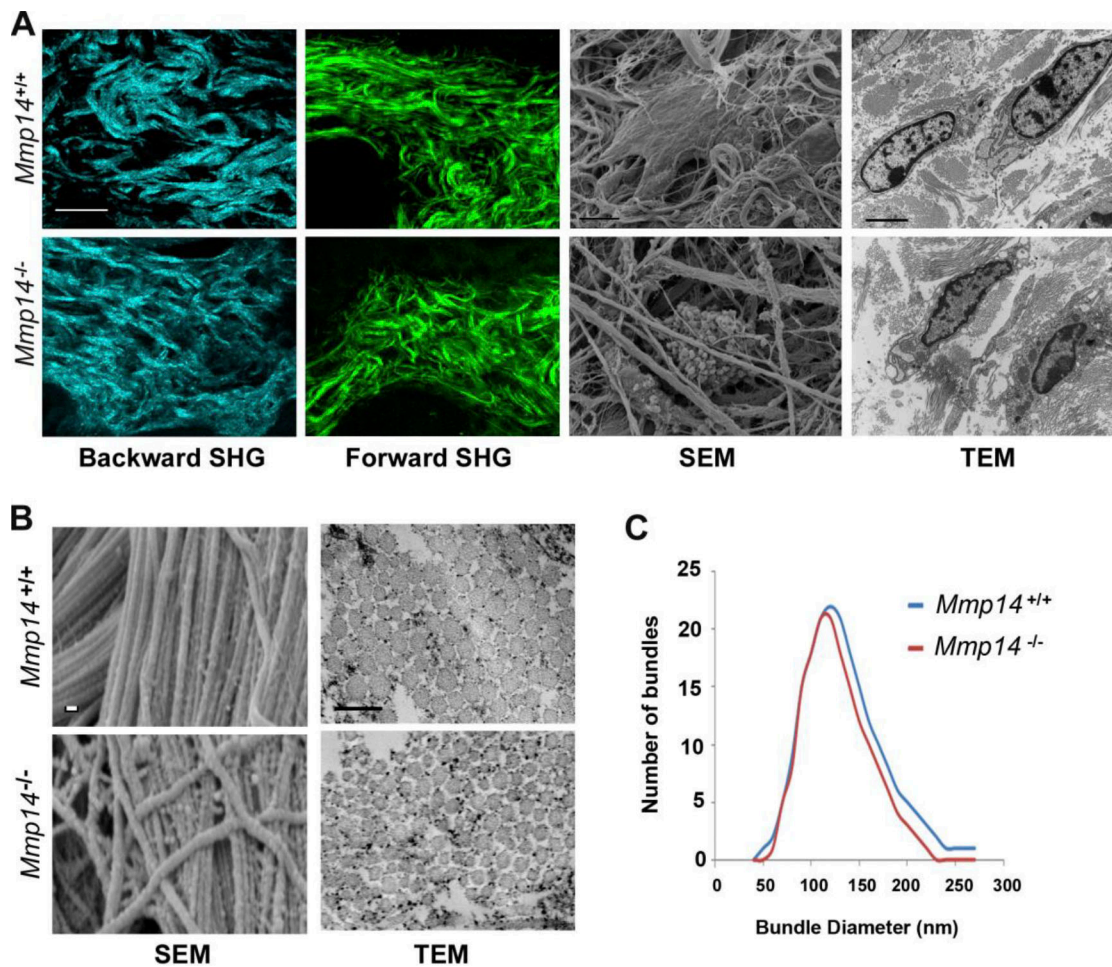


Figure S4. **Postnatal maturation of the dermal extracellular matrix.** (A) Second harmonic generation (SHG) imaging (backward and forward scatter) of type I collagen in skin cross-sections recovered from 2-wk-old *Mmp14^{+/+}* or *Mmp14^{-/-}* mice (bar = 20 μ m). SEM and TEM imaging of the dermis illustrates an extensive array of collagen bundles surrounding fibroblasts (bar = 2 μ m). (B) Higher magnification of SEM and TEM images highlight similar architecture of collagen bundles and size in dermal tissue recovered *Mmp14^{+/+}* and *Mmp14^{-/-}* mice (SEM, bar = 1 μ m; TEM, bar = 200 nm). (C) Diameter of collagen fibers was quantified in five random fields of captured TEM images in a wild-type versus a null littermate. Results are representative of two experiments.

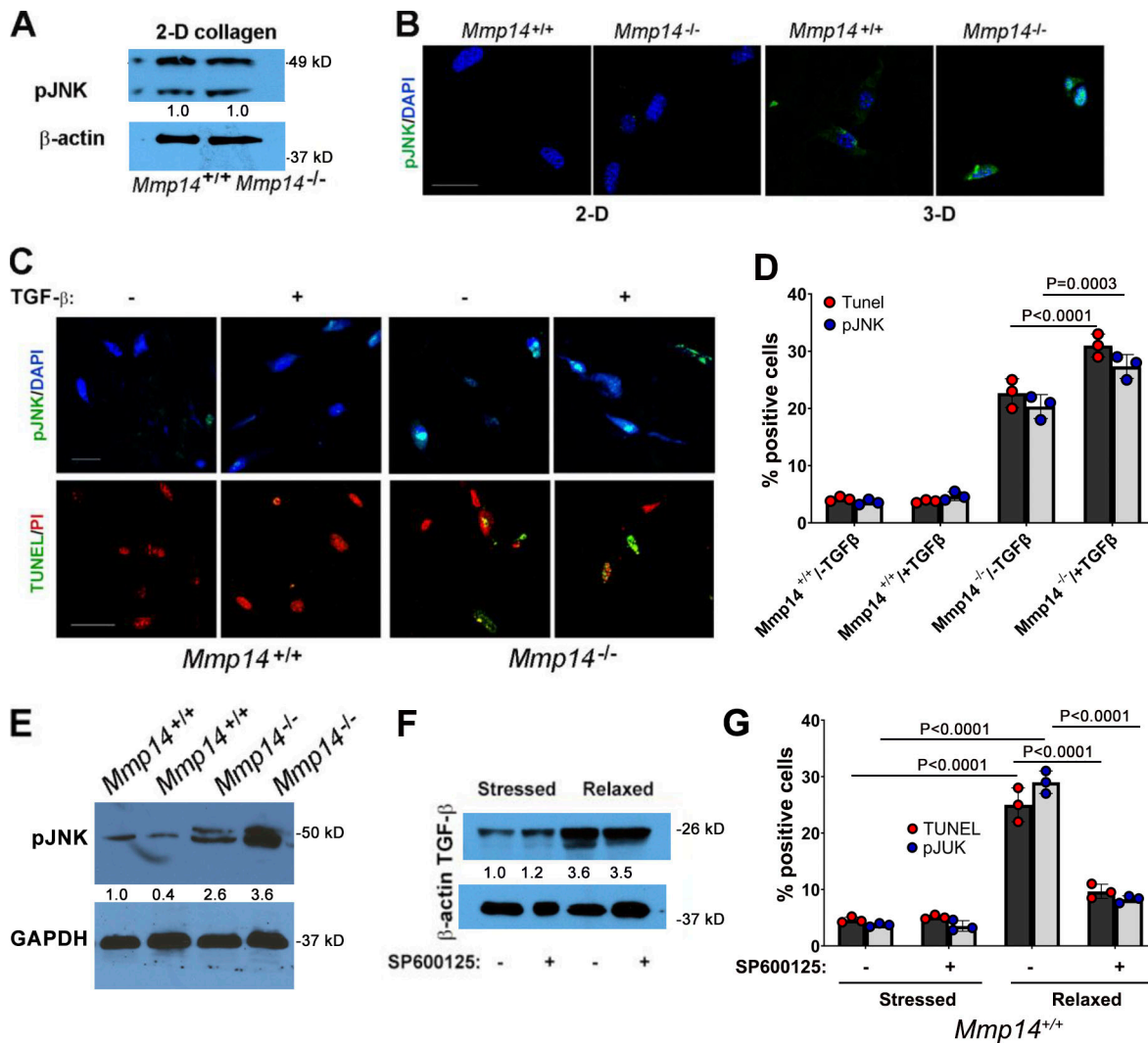


Figure S5. **A TGF- β /JNK cascade induces fibroblast apoptosis.** (A) Western blot of pJNK expression levels as assessed by western blot in lysates prepared from *Mmp14*^{+/+} or *Mmp14*^{-/-} fibroblasts cultured atop (2-D) type I collagen hydrogels with β -actin used as the loading control. Results representative of two experiments performed. Relative expression levels are shown as determined by densitometry. (B) pJNK immunostaining and TUNEL staining of wild-type versus null fibroblasts in 2-D relative to 3-D collagen hydrogel culture (bar = 25 μ m). Results representative of three experiments performed. (C and D) *Mmp14*^{+/+} or *Mmp14*^{-/-} fibroblasts were embedded in collagen hydrogels in the absence or presence of exogenous TGF- β 1 (10 ng/ml) for 5 days with JNK activation and TUNEL staining monitored by fluorescent imaging (bar = 25 μ m) (C) and quantified in D (mean \pm SEM; *n* = 3 independent experiments). Two-way ANOVA and Tukey post-test. (E) pJNK levels in dermal tissue lysates recovered from 3-wk-old wild-type versus *Mmp14*^{-/-} mice (*n* = 2). Relative expression levels are shown as determined by densitometry. (F) TGF- β protein levels in 3-D cultures of *Mmp14*^{+/+} fibroblasts under stressed or stressed/relaxed conditions in the absence or presence of SP600125 as assessed by western blot. Results representative of three experiments performed. Relative expression levels are shown as determined by densitometry. (G) *Mmp14*^{+/+} fibroblasts were cultured in 3-D collagen hydrogels under stressed or stressed/relaxed conditions in the absence or presence of SP600125 and the number of pJNK- and TUNEL-positive cell quantified in five or more randomly selected cross-sections of the gel in three independent experiments (mean \pm SEM). Two-way ANOVA and Tukey post-test. Source data are available for this figure: SourceData F55.

Dermal fibroblasts

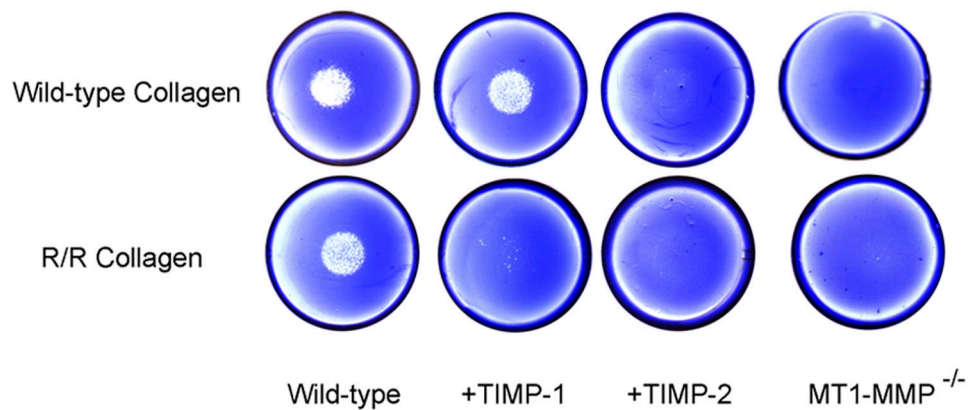


Figure S6. **Fibroblast-mediated degradation of r/r collagen.** Mouse dermal fibroblasts recovered from wild-type or *Mmp14* knockout mice were cultured atop acid-solubilized mouse tail wild-type or r/r type I collagen matrices for 48 h in the absence or presence of 5 μ g of TIMP-1 or TIMP-2 for 48 h. At the end of the culture period, fibroblasts were lysed and the collagen gel stained and destained with Coomassie blue. Wild-type, but not *Mmp14* knockout, fibroblasts degraded the subjacent wild-type collagen matrix via a process sensitive to TIMP-2, but not TIMP-1. By contrast, wild-type, but not *Mmp14* knockout, fibroblasts degraded r/r collagen via a process inhibitable by both TIMP-1 and TIMP-2. Results representative of four independent experiments.

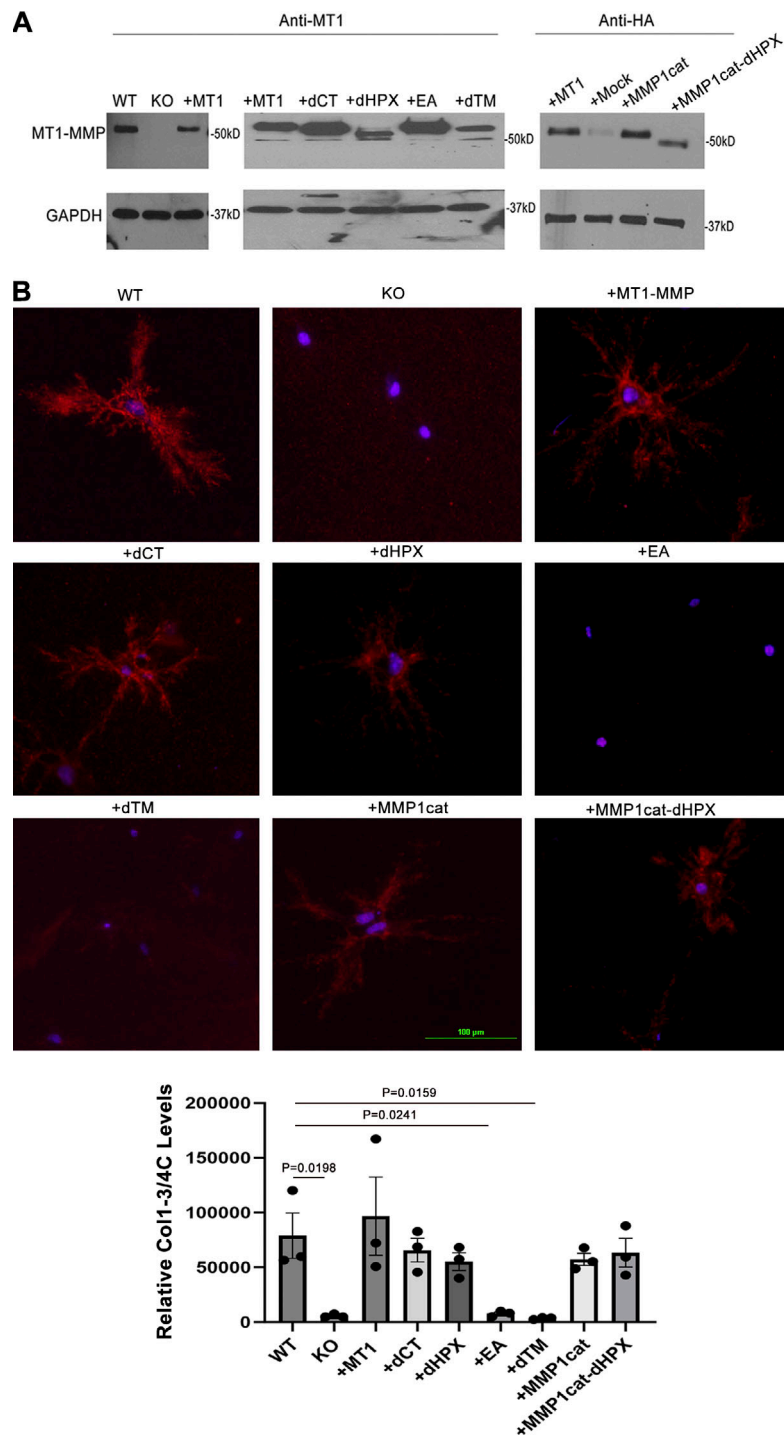


Figure S7. **Expression and collagenolytic activity of MMP14 mutant constructs.** (A) Wild-type, Mmp14-null, or transduced Mmp14-null fibroblasts expressing various MMP14 expression vectors were subjected to western blot analysis with a polyclonal anti-MT1-MMP antibody directed against the catalytic domain of MMP14 or an anti-HA antibody to detect HA-tagged MMP14 mutant constructs. Following transduction, Mmp14-null fibroblasts expressed MT1-MMP at levels comparable to wild-type levels of endogenous Mmp14 (far left panel). In the middle panel, Mmp14-null fibroblasts were transduced with each of the listed mutants, demonstrating comparable expression levels, save for the transmembrane-deleted construct (dTM) where the bulk of the protein is secreted into the medium. In the far right panel, Mmp14 knockout fibroblasts were transduced with HA-tagged MT1-MMP or HA-tagged MMP1 chimera expression vectors (the polyclonal MT1-MMP antibody used in the preceding blots is primarily directed against the MT1-MMP catalytic domain, which has been replaced with that of MMP1). In this case, both of the MMP1 chimeric mutants, with or without the Mmp14 hemopexin domain, are expressed at near normal levels. Results are representative of two or more experiments performed. (B) Wild-type (WT), Mmp14 knockout (KO), or transduced Mmp14 mouse dermal fibroblasts were embedded in 3-D type I collagen hydrogels and cultured for 48 h. At the end of the culture period, Col1 3/4C staining was performed and degradation quantified using ImageJ (bar = 100 μ m). Immunostaining results are representative of three independent experiments performed while degradation results are presented as the mean \pm SEM of three independent experiments. One-way ANOVA and Dunnett post-test. Source data are available for this figure: SourceData FS7.

Provided online is Table S1, which shows the matrix metalloproteinase count data summary.